University of Szeged
Albert Szent-Györgyi Medical School
Doctoral School of Experimental and Preventive Medicine

ORGANOSULFUR COMPOUNDS AMELIORATE THE SEVERITY OF EXPERIMENTAL ACUTE PANCREATITIS AND EXERT CYTOPROTECTION

Ph.D. Thesis

Erik Márk Orján, M.Sc.

Supervisor:
Lóránd Kiss Ph.D.

Szeged,
2026

PUBLICATIONS

Publications related to the subject of the thesis

Orján EM, Kormányos ES, Fűr GM, Dombi Á, Bálint ER, Balla Z, Balog BA, Dágó Á, Totonji A, Bátai ZI, Jurányi EP, Ditrói T, Al-Omari A, Pozsgai G, Kormos V, Nagy P, Pintér E, Rakonczay Z Jr, Kiss L. The anti-inflammatory effect of dimethyl trisulfide in experimental acute pancreatitis. Sci Rep. 2023; 13(1):16813. doi: 10.1038/s41598-023-43692-9. [IF_{2023}: 3.8], **D1**

Orján EM, Dágó Á, Sándor B, Salamah O, Mihalekné Fűr G, Balog BA, Rakonczay Z Jr, Kiss L. Investigation of organosulfur molecules in experimental acute pancreatitis: Antioxidant and antiferroptotic actions of ATB-346. Biomed Pharmacother. 2026; 196:119089. doi: 10.1016/j.biopha.2026.119089. [IF_{2024}: 7.5**], **D1**

** *On the Norwegian list of journals*

Publications not related to the subject of the thesis

Bálint ER, Fűr G, Kui B, Balla Z, Kormányos ES, **Orján EM**, Tóth B, Horváth G, Szűcs E, Benyhe S, Ducza E, Pallagi P, Maléth J, Venglovecz V, Hegyi P, Kiss L, Rakonczay Z Jr. Fentanyl but Not Morphine or Buprenorphine Improves the Severity of Necrotizing Acute Pancreatitis in Rats. Int J Mol Sci. 2022; 23(3):1192. doi: 10.3390/ijms23031192. [IF_{2022}: 5.6], **Q1**

Balla Z, Kormányos ES, Kui B, Bálint ER, Fűr G, **Orján EM**, Iványi B, Vécsei L, Fülöp F, Varga G, Harazin A, Tubak V, Deli MA, Papp C, Gácser A, Madácsy T, Venglovecz V, Maléth J, Hegyi P, Kiss L, Rakonczay Z Jr. Kynurenic Acid and Its Analogue SZR-72 Ameliorate the Severity of Experimental Acute Necrotizing Pancreatitis. Front Immunol. 2021; 12:702764. doi: 10.3389/fimmu.2021.702764. [IF_{2021}: 8.787], **Q1**

Fűr G, Bálint ER, **Orján EM**, Balla Z, Kormányos ES, Czira B, Szűcs A, Kovács DP, Pallagi P, Maléth J, Venglovecz V, Hegyi P, Kiss L, Rakonczay Z Jr. Mislocalization of CFTR expression in acute pancreatitis and the beneficial effects of VX-661/VX-770 treatment on disease severity. J Physiol. 599, 4955-4971. doi: 10.1113/JP281765. [IF_{2021}: 6.228], **Q1**

Tasi DA, **Orján EM**, Czakó G. Benchmark Ab Initio Mapping of the F^- + CH_2ClI S_N2 and Proton-Abstraction Reactions. J Phys Chem A. 2024; 128(49):10568-10578. doi: 10.1021/acs.jpca.4c06716. [IF_{2024}: 2.8], **Q2**

Orján EM, Nacsa AB, Czakó G. Conformers of dehydrogenated glycine isomers. J Comput Chem. 2020; 41(22):2001-2014. doi: 10.1002/jcc.26375. [IF_{2020}: 3.376], **Q1**

Scientometrics

https://m2.mtmt.hu/gui2/?type=authors&mode=browse&sel=10073212&view=pubTable

Number of publications:	7
Publications with first authorship:	3
Cumulative impact factor:	30.591
Ranking (Sci Mago):	D1: 2, Q1: 4, Q2: 1
Number of independent citations (MTMT2):	36
Hirsch index:	4

LIST OF ABBREVIATIONS

ACh – acetylcholine

AP – acute pancreatitis

Cer – cerulein

CBS – cystathionine β-synthase

CDC – chenodeoxycholate

CTH – cystathionine -γ-lyase

DATS – diallyl trisulfide

DMSO – dimethyl sulfoxide

DMTS – dimethyl trisulfide

EtOH-POA –ethanol and palmitoleic acid

GAPDH – glyceraldehyde-3-phosphate dehydrogenase

GPX4 – glutathione peroxidase 4

GSH – glutathione

ic[Ca^{2+}] – intracellular Ca^{2+} concentration

LC-MS/MS – liquid chromatography-tandem mass spectrometry

L-arg – L-arginine-HCl

MDA – malondialdehyde

MPO – myeloperoxidase

MTT – 3-(4,5-dimethylthiazol-2-yl)-2,5-diphenyltetrazolium bromide

NF-κB – nuclear factor κB

Nrf2 – nuclear factor-erythroid 2 related factor 2

NSAID – non-steroidal anti-inflammatory drug

PI – propidium iodide

Poly80 – polysorbate 80

PS – physiological saline

ROS – reactive oxygen species

SDS – sodium dodecyl sulfate

TABLE OF CONTENTS

INTRODUCTION

I. The physiology of the pancreas

The pancreas is a retroperitoneal gland of the gastrointestinal tract located in the upper abdomen and possesses both exocrine and endocrine functions. The endocrine component comprises the islets of Langerhans and is responsible for the synthesis and secretion of various hormones, such as glucagon, insulin, and pancreatic polypeptide, which are vital for the regulation of the body's metabolism. The exocrine pancreas consists primarily of acinar and ductal epithelial cells, and its function is to produce pancreatic juice, a mixture of digestive enzymes and electrolyte-rich fluid [1]. Acinar cells account for more than 80% of the organ's tissue and synthesise, store, and excrete digestive enzymes as inactive precursors (zymogens), which become active in the duodenum. Zymogens are secreted in an isotonic, NaCl- and H^+-rich fluid from which Cl^- is then exchanged for HCO_3^- by ductal cells [2]. The resulting high HCO_3^- concentration (up to 140 mM) ensures that the secretion maintains an alkaline pH, thereby neutralising the acid chyme from the stomach and providing an optimal pH in the intestinal lumen for enzyme activity [3]. Approximately 1.5–2 litres of pancreatic juice are secreted daily into the duodenum to flush down the digestive enzymes and prevent their premature activation. In the duodenum, enterokinase catalyses the conversion of trypsinogen to trypsin, initiating an activation cascade. The resulting trypsin then further activates trypsinogen and converts all other proenzymes into their active forms.

II. Acute pancreatitis

II.1. Definition, epidemiology, classification, and aetiology

Acute pancreatitis (AP) is a sudden inflammatory disease of the exocrine pancreas and is a leading cause of non-malignant gastrointestinal-related hospitalisation [4]. Although the overall mortality is ~2 %, approximately 20 % of patients will develop a more severe form of AP associated with organ failure, in which the mortality can reach 30 % [5]. The annual incidence of the disease exceeds 30/100,000 population and shows an increasing tendency in developed countries [6].

AP typically presents with sudden, severe epigastric pain radiating to the back, often accompanied by nausea and vomiting. The severity of the disease varies widely and can be categorised as mild, moderately severe, or severe forms based on the Revised Atlanta Classification system [7]. Mild AP is limited to the pancreas and has no local complications or organ failure. The majority of AP cases are mild, and patients typically recover within a week.

Moderately severe AP resolves more slowly and is associated with local (e.g. peripancreatic fluid accumulation, pseudocyst, necrosis) or systemic complications, accompanied by transient organ failure that resolves within 48 hours. Severe AP is characterised by persistent organ failure lasting more than 48 hours. The most commonly affected extrapancreatic organs in AP are the lungs, heart, and kidneys. Approximately 25–30% of patients experience recurrent episodes of AP, which carries a significant risk of progression to chronic pancreatitis or pancreatic cancer. The diagnosis of AP requires at least two of the following three criteria: (i) characteristic symptoms (epigastric upper abdominal pain); (ii) elevated serum lipase activity (or amylase activity), at least three times greater than the upper limit of normal; (iii) imaging consistent with the diagnosis [8].

The most common causes of AP include gallstones, alcohol consumption, and hypertriglyceridemia (HTG). Biliary pancreatitis and alcohol-induced AP account for about 60–80 % of AP cases, whereas AP induced by HTG with serum triglyceride levels above 11.3 mM is less common (approximately 9 %) [9]. Biliary pancreatitis may occur when a gallstone obstructs either the bile duct or the pancreatic duct [10]. Alcohol-induced AP is characterised by regular and excessive alcohol consumption, often accompanied by a high-fat diet [11]. HTG-induced AP is associated with demographic factors (e.g. younger age, higher male predominance) and a history of obesity or type-2 diabetes mellitus [12]. Less common causes of AP include endoscopic retrograde cholangiopancreatography, hypercalcemia, genetic polymorphisms, toxins, and drugs.

II.2. Pathogenesis

The pathomechanism of the disease is complex and not yet fully understood. The disruption of normal intracellular Ca^{2+} signalling, a key mechanism of AP, triggers the premature activation of digestive enzymes by blocking the secretion of zymogens into the ductal space and by promoting the colocalization of proenzymes with lysosomal enzymes, such as cathepsin B (Fig. 1) [13,14]. Under physiological conditions, the inositol trisphosphate receptor and ryanodine receptor Ca^{2+} release channels on the endoplasmic reticulum (ER), the store-operated Ca^{2+} channels on the plasma membrane, and several two-pore channels are sources of global and sustained Ca^{2+} influx. Prolonged ER Ca^{2+} release and cellular Ca^{2+} entry, due to continued toxic stimulation, overload the mitochondria and trigger the opening of the mitochondrial permeability transition pore, leading to the loss of mitochondrial membrane potential [15]. Disruption of mitochondrial membrane function results in the release of mitochondrial contents (e.g. cytochrome c) and a low-energy state due to ATP depletion.

Decreased ATP production impairs Ca^{2+} clearance, thereby facilitating sustained and peaked cytosolic Ca^{2+} concentrations.

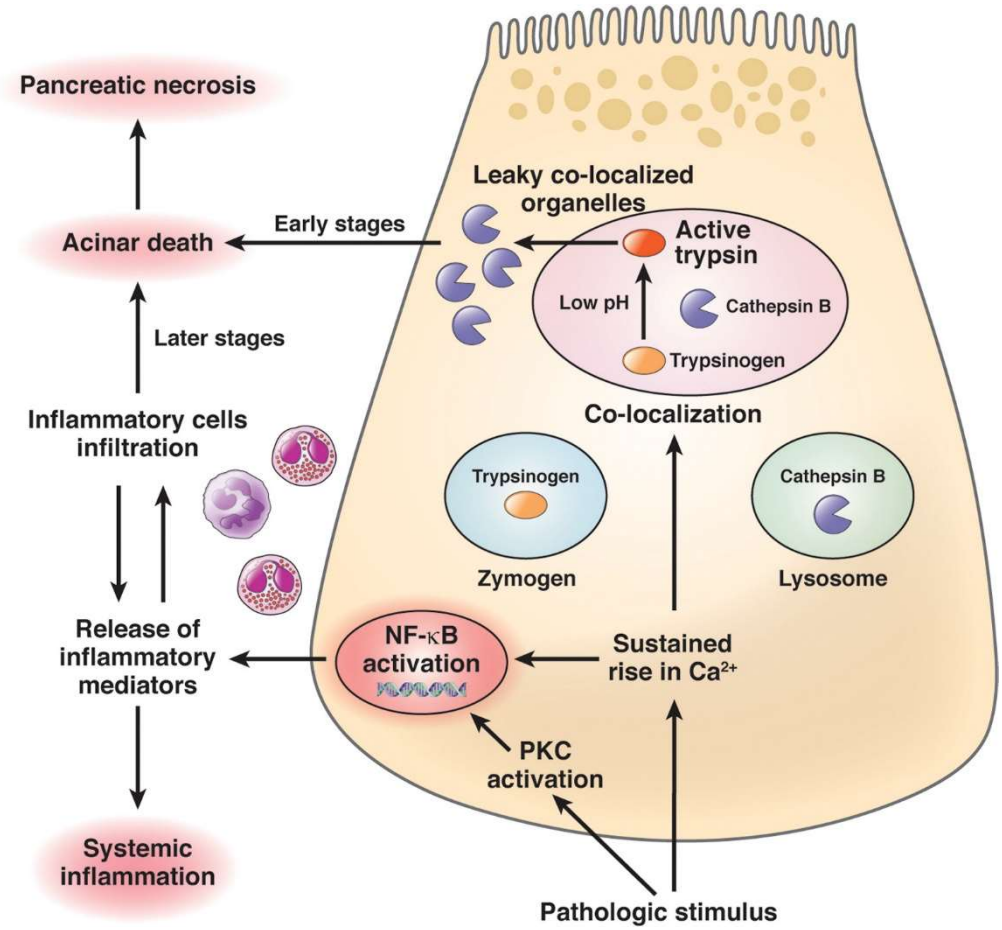

FIG 1. The pathogenesis of acute pancreatitis. The disruption of normal intracellular Ca^{2+} signalling by a pathological stimulus initiates the premature activation of digestive enzymes and the activation of nuclear factor κB (NF-κB). The colocalisation of lysosomal and zymogen compartments leads to cathepsin B leakage into the cytosol, resulting in premature activation of trypsinogen and, consequently, acinar cell death in the early stages of pancreatitis. The activation of NF-κB occurs independently of trypsinogen activation and leads to the release of inflammatory mediators, as well as the recruitment of inflammatory cells. These processes contribute to acinar cell death in the later stages of pancreatitis and drive the systemic inflammatory response. Abbreviations: PKC, protein kinase C. Source: Saluja et al., 2019.

Independent of trypsinogen activation, pathologic Ca^{2+} signalling also induces the translocation of nuclear factor κB (NF-κB) into the nucleus, and NF-κB activation leads to the release of cytokines (e.g. interleukins 1 and 6, tumour necrosis factor-α), which contribute to leukocyte recruitment and promote the inflammatory response [16,17]. Among the first immune cells recruited into the pancreas, neutrophils produce numerous enzymes (e.g. myeloperoxidase – MPO), chemokines, and cytokines, while also activating additional intrapancreatic digestive enzymes [18]. Damage-associated molecular patterns (e.g. ATP, cytokines) are released from damaged and necrotic cells and can induce further inflammation. In addition, the intra-acinar

generation of reactive oxygen species (ROS) increases with the decreasing capacity for systemic clearance [19]. Excessive ROS accumulation and ATP depletion promote necrosis, a hallmark of the severe form of the disease [20].

Other critical cellular processes during AP include impaired autophagy, ER stress, and decreased ductal HCO_3^- and fluid secretion [13]. The reduced ductal function further aggravates the early enzyme activation and acinar cell damage. Low concentrations of AP-triggering factors (alcohol or bile acids) stimulate, whereas high concentrations inhibit HCO_3^- secretion. In addition, pancreatic duct obstruction can alter acinar cell membrane trafficking, thereby facilitating the progression of AP. Decreased lysosomal functions and altered maturation of lysosomal hydrolases have been shown to impair autophagy, leading to mitochondrial dysfunction, ER stress, dysregulated lipid metabolism, and increased AP severity (Fig. 1). ER stress is known to disrupt the physiologic apical secretory process and may be associated with the development of an autophagic response and the colocalisation of zymogens with lysosomal enzymes, both of which are directly known to lead to trypsinogen activation [15]. Although many of the critical pathways of AP have been identified, unfortunately, the disease's management is still based on supportive therapy.

II.3. Ferroptosis and its role in AP

During the pathogenesis of AP, acinar cells are damaged and die via various cell death pathways, including necrosis, apoptosis, necroptosis, ferroptosis, and pyroptosis [21]. The type of cell death can determine the severity of the disease, and necrosis, necroptosis, and ferroptosis are associated with the severe forms of AP. Ferroptosis is an iron-dependent, non-apoptotic form of programmed cell death, characterised by the accumulation of iron and the extensive production of ROS and lipid peroxides [22]. Iron can trigger ROS generation by initiating the Fenton reaction and acts as a cofactor for lipid peroxidase enzymes [23,24]. Antioxidant systems, such as glutathione peroxidase 4 (GPX4) and its cofactor glutathione (GSH), convert phospholipid peroxides into non-toxic lipid alcohols and provide resistance to ferroptosis [25,26]. Previous reports have demonstrated that iron accumulation in AP may upregulate ferroptosis-related proteins in the pancreas, and that early trypsin activation can degrade the GPX4 enzyme [27,28]. Deregulated autophagy was also shown to initiate ferroptosis by degrading ferritin, the primary iron ion-storing protein, leading to oxidative injury [29]. Increased lipid peroxidation can activate multiple inflammatory pathways, and the release of pro-inflammatory mediators will further exacerbate lipid peroxidation and intracellular oxidative stress, suggesting a close relationship between ferroptosis and inflammation [30,31].

III. Endogenous hydrogen sulfide

Hydrogen sulfide (H_2S) is recognised as a signalling molecule that appears to regulate diverse cellular physiological processes, and alterations in endogenous H_2S synthesis have been associated with the development of various diseases [32,33]. In mammalian cells, H_2S is produced mainly from L-cysteine and homocysteine by three enzymes: cystathionine β-synthase (CBS), cystathionine γ-lyase (CTH), and 3-mercaptopyruvate sulfurtransferase. All three enzymes are widely distributed across tissues but differ in their locations and expression levels. In addition to the enzymatic synthesis of H_2S, there exist bound sulfur sources capable of releasing free H_2S upon acidification or reduction of the parent molecule.

Emerging research indicates that H_2S reduces oxidative stress and exerts cytoprotective effects by scavenging ROS and enhancing antioxidant enzyme activity [34,35]. Reduced H_2S production has been described in various conditions, including atherosclerosis, hypertension, and hepatic steatosis [36–38]. Conversely, its protective role has been shown in Alzheimer's and Parkinson's diseases, ischaemia-reperfusion injury, diabetes mellitus, and arthritis. Its complex interaction with lipid peroxides, as well as its ability to promote GPX4 expression, also emphasises its role in preventing ferroptotic processes [34,39]. Currently, more than 300 clinical trials (ClinicalTrials.gov) are associated with H_2S research, emphasising its significant translational potential.

Although the upregulation of H_2S synthesis or its administration confers protective effects in inflammatory conditions, the overexpression of enzymes responsible for H_2S production may exacerbate inflammation through the activation of NF-κB [40]. Whiteman et al. demonstrated that the rapid release of H_2S at high concentrations exhibits pro-inflammatory effects, indicating that both the absolute concentration of H_2S and the time course of its presence following inflammation induction are of critical importance [41]. While the physiological and pathophysiological effects of H_2S have been extensively investigated, many questions and apparent contradictions remain regarding how it acts in living organisms.

IV. Organosulfur molecules

Sulfur-containing organic compounds, known as organosulfurs, are abundantly found in nature (e.g. cysteine, biotin, penicillin), and synthetic ones also exist. Many of them are biologically active and can influence specific signalling pathways (e.g. NF-κB, nuclear factor-erythroid 2 related factor 2 – Nrf2), activate ion channels (K^+, Ca^{2+}, transient receptor potential ankyrin – TRPA, or transient receptor potential vanilloid channels), affect protein function

through persulfidation, and exhibit antioxidant properties [42–45]. Numerous organosulfur compounds are also potential H_2S donors, and their anti-inflammatory effects are most probably linked to H_2S release.

Organosulfurs and H_2S donors, such as S-diclofenac, S-propargyl-cysteine, and sulforaphane, have been shown to attenuate the severity of AP and/or the associated lung injury [40,46–48]. Administration of diallyl disulfide, a garlic-derived organosulfur compound, significantly ameliorated the pancreatic tissue injury and the damage in the lungs resulting from AP. Its anti-inflammatory effect was associated with decreased serum amylase activity, tumour necrosis factor-α, preprotachykinin A, and neurokinin-1 receptor expression, as well as H_2S production in both the pancreas and the lung [49]. Other organosulfurs, namely dimethyl trisulfide (DMTS), diallyl trisulfide (DATS), GYY4137, AP39, and ATB-346, have been reported to exhibit very strong anti-inflammatory and antioxidant effects across various disease conditions, but no information exists regarding their impact on AP.

IV.1. DMTS

DMTS is a naturally occurring organosulfur compound and the simplest organic trisulfide. It reacts with haemoglobin, facilitating methaemoglobin formation, and also has a great potential to reduce cyanide poisoning [50,51]. DMTS was also shown to activate the TRPA1 ion channel, a Ca^{2+} channel that acts as a sensor for pain, modulate pain sensation, and reduce inflammation in serum-transfer arthritis [52,53].

IV.2. DATS

DATS is a natural H_2S donor organosulfur that can be metabolised by GSH in erythrocytes to form H_2S at a consistent rate over a prolonged period of time. Lee et al. showed that DATS suppresses the activation of the NF-κB signalling pathway and inhibits lipopolysaccharide binding to Toll-like receptor 4 in macrophages [45]. It also exhibited antioxidant activity by mitigating oxidative stress and augmenting the activity of antioxidant enzymes (e.g. superoxide dismutase – SOD) [54–56].

IV.3. GYY4137

GYY4137 is a synthetic, water-soluble H_2S donor organosulfur molecule, designed to release H_2S in a gradual and sustained manner. Previous research has demonstrated its ability to decrease the levels of pro-inflammatory cytokines (e.g. interleukins 1 and 6, tumour necrosis factor-α) and to reduce the secretion of nitric oxide and prostaglandin E2 [57]. GYY4137 was also shown to induce apoptosis and possess potent anti-cancer activity [58,59].

IV.4. AP39

AP39 is a synthetic, slow-releasing H_2S donor organosulfur compound with mitochondria-targeting capabilities. The molecule comprises a triphenylphosphonium cation linked to an H_2S donor by an aliphatic linker, enabling it to accumulate in the mitochondria. AP39 has been shown to protect endothelial cells during oxidative stress and maintain mitochondrial DNA integrity [60]. It also limited mucosal injury and altered the tissue inflammatory response in necrotising enterocolitis [61].

IV.5. ATB-346

Due to severe side effects caused by non-steroidal anti-inflammatory drugs (NSAIDs) in the gastrointestinal tract, novel H_2S-releasing derivatives were developed to provide gastrointestinal safety while maintaining or exceeding the efficacy of their parent drugs in pain modulation and inflammation [62–64]. ATB-346 combines a traditional NSAID, naproxen, with a covalently attached H_2S-donor chemical moiety, 4-hydroxy-thiobenzamide. It has demonstrated anti-inflammatory effects in various inflammatory diseases by reducing several inflammatory parameters, including pro-inflammatory cytokine expression, leukocyte infiltration, and cyclooxygenase activity [44,65]. Dief et al. showed that ATB-346 suppresses neutrophil adherence and exhibits chondroprotection in a rat model of zymosan-induced arthritis [66]. It also reduced inflammation in humans in a model of acute dermal inflammation and provided evidence of significant protection against the development of gastrointestinal ulcers in a Phase 2B clinical study [67,68].

AIMS

Given the significant anti-inflammatory potential of organosulfur compounds, our objective was to comprehensively investigate and compare the five most widely studied organosulfur molecules in experimental AP: ATB-346, DMTS, DATS, GYY4137, and AP39. Furthermore, we aimed to provide insights into the mechanisms of action of DMTS and ATB-346 in both *in vivo* and *in vitro* studies. Our detailed aims were the following:

1) to compare the five aforementioned organosulfurs as therapeutic agents against experimental AP both *in vivo* (mice) and *in vitro* (pancreatic acinar cells)
2) to reveal how DMTS influences the severity of AP by investigating its effect on oxidative stress, cellular viability, and intracellular Ca^{2+} signalling, as well as by assessing its impact on serum and tissue sulfide levels
3) to investigate the impact of ATB-346 on AP severity by testing its effect on oxidative stress and ferroptosis

MATERIALS AND METHODS

I. Materials and solutions

All chemicals were obtained from Merck Life Science Kft. (Budapest, Hungary) unless indicated otherwise. The solutions utilised for *in vivo* measurements were freshly prepared before each experiment. Cerulein (Cer) (Glentham Life Sciences, Corsham, UK) was dissolved in dimethyl sulfoxide (DMSO), and the working solution (5 µg/mL) was diluted in physiological saline (PS). Palmitoleic acid (POA) was dissolved in absolute ethanol (EtOH) (87.67 mg/mL working solution). The organosulfur solutions were prepared in the following manner: (1) ATB-346 (Cayman Chemical, Ann Arbor, MI, USA) was dissolved in DMSO (200 mM stock solution) and the solution was diluted to 5 mM in 50 mg/ml polysorbate 80 (Poly80) in PS by stirring overnight; (2) AP39 (Cayman Chemical, Ann Arbor, MI, USA) was prepared in DMSO (20 mM stock solution) and then further diluted to 20 µM in PS; (3) GYY4137 (Cayman Chemical, Ann Arbor, MI, USA) was dissolved in PS (5 mM); (4) DATS (Cayman Chemical, Ann Arbor, MI, USA) was prepared in 50 mg/mL Poly80 in PS (50 mM) by stirring overnight; (5) DMTS was dissolved in 30 mg/mL Poly80 in PS (79.2 mM) by stirring overnight. Antibodies used for Western blotting, the tissue culture media and the Malondialdehyde (MDA) Colourimetric Assay Kit were purchased from Thermo Fisher Scientific (Waltham, MA, USA)

II. Animals

Eight- to ten-week-old male FVB/N mice weighing 22–30 g were used for the experiments. The animals were obtained from Charles River Laboratories Inc. (Wilmington, MA, USA). They were housed in the departmental animal facility at a constant room temperature of 24°C with a 12-hour light-dark cycle and were allowed free access to water and standard laboratory chow for rodents (Innovo Kft., Isaszeg, Hungary).

The experiments were conducted in accordance with the European Union Directive 2010/63/EU and the Hungarian Government Decree 40/2013 (II.14.). Experiments involving animals were approved by both local (University of Szeged) and national ethical committees (permit no. X./1714/2020).

III. *In vivo* experiments: acute pancreatitis induction, treatment with organosulfurs and tissue harvesting

All *in vivo* experiments were performed in a dedicated laboratory space. The animals were randomly allocated into groups using a computer-based random order generator. No criteria for inclusion and exclusion were set. In the first part of the study, necrotising AP was induced by intraperitoneal (i.p.) hourly injections of 10 × 50 μg/kg Cer. The different organosulfur treatment doses, administration routes and timing are shown in Table 1. For DMTS and ATB-346, we employed another necrotising AP model. Here, AP was induced by i.p. hourly injections of 2 × 1.35 g/kg EtOH and 2 × 150 mg/kg POA in mice.

Control groups were given PS instead of Cer or EtOH-POA, and Poly80, DMSO or the combination of Poly80 and DMSO instead of the corresponding organosulfur. The animals were sacrificed 12 h after the first Cer injection or 24 h after the first EtOH-POA by deep anaesthesia induced with 150 mg/kg i.p. pentobarbital (Bimeda MTC, Cambridge, Canada). These time points refer to generally accepted timings when Cer-AP or EtOH-POA-AP reaches the peak severity of the disease. Immediately after opening the abdomen, a small piece of the pancreas was removed and transferred to TRI-reagent (Zymo Research, Irvine, CA, USA) for subsequent mRNA expression analysis. Blood was collected via cardiac puncture (~400 μL) and allowed to clot at 0°C for 30 min. Following centrifugation (3,500 g at 4ºC for 15 min), the serum was obtained and stored at –20°C until use. The pancreas was rapidly removed and cleaned of fat and lymph nodes on ice, then cut into pieces. One large portion was promptly frozen in liquid nitrogen and stored at –80°C until biochemical assays were conducted. Another piece of the pancreas was fixed in 8 % neutral formaldehyde solution for histological analysis. A third part was stored in Eppendorf tubes at room temperature for dry-wet weight measurement. To minimise subjective biases, various investigators were involved at different stages of each *in vivo* experiment (allocation and administering of the treatments, animal sacrifice, outcome assessment, and data analysis).

Table 1. Organosulfur treatment doses, administration routes, and timing.

Organosulfur / *AP models*	**DMTS**		**DATS**	**GYY4137**	**AP39**	**ATB-346**	
	Cer AP	*EtOH-POA AP*	*Cer AP*	*Cer AP*	*Cer AP*	*Cer AP*	*EtOH-POA AP*
Administration routes	*s.c.*	*s.c.*	*i.p.*	*i.p.*	*i.p.*	*p.o.*	*p.o.*
Doses (µmol/kg)	2 × 400 2 × 600 2 × 800	3 × 600 3 × 800	2 × 25 2 × 50 2 × 100	2 × 25 2 × 50 2 × 100	2 × 0.125 2 × 0.25 2 × 0.5	2 × 20 2 × 40 2 × 80	3 × 40 3 × 80
Timing of the treatments (hours from the first Cer or EtOH-POA injection)	2, 5 or 0, 3	1, 6, 12 or 0, 3 12	2, 5	2, 5	2, 5	2, 5	2, 6, 12

Abbreviations: AP, acute pancreatitis; DMTS, dimethyl trisulfide; DATS, diallyl trisulfide; Cer, cerulein; EtOH-POA, ethanol and palmitoleic acid; s.c., subcutaneous; i.p., intraperitoneal; p.o., per os.

IV. Histological analysis

The formalin-fixed pancreatic samples were dehydrated and cleaned before being paraffin-embedded and sectioned to 3 µm. These sections were stained with hematoxylin and eosin and were evaluated by two independent, blinded observers. Oedema was scored between 0 and 3 points (0: none; 1: patchy interlobular; 2: diffuse interlobular; 3: diffuse interlobular and inter-acinar), leukocyte infiltration between 0 and 4 points (0: none; 1: patchy interlobular; 2: mild diffuse interlobular; 3: moderate diffuse interlobular; 4: diffuse interlobular and intra-acinar) [69]. The percentage of cell damage was also assessed, with all forms of cell death (necrosis and apoptosis) classified as tissue damage.

V. Laboratory measurements

To evaluate pancreatic water content, the wet weight (WW) of the pancreas was measured immediately after harvesting. The tissues were then dried for 48 h at 100°C, and the dry weight (DW) was also measured. The wet/dry weight ratio was calculated as [(WW–DW)/WW] × 100.

Serum amylase activity was measured on a FLUOstar OPTIMA microplate reader (BMG Labtech, Ortenberg, Germany) using a colourimetric kinetic method and a commercial amylase activity kit (Diagnosticum Zrt., Budapest, Hungary). The absorbance of the samples was detected at 405 nm.

Pancreatic MPO activity, a hallmark of neutrophil granulocyte infiltration, was also determined. Briefly, pancreatic tissues (~50 – 100 mg) were thawed and chopped into small pieces before being homogenised in phosphate buffer (20 mM KH_2PO_4 and 20 mM K_2HPO_4 buffer, pH = 7.4) using an ultrasonic homogeniser (Branson Sonifier 250; Emerson Electric, Brookfield, CT, USA). on ice. After centrifugation (20,000 g at 4ºC for 20 min), the pellets were collected and resolved in phosphate buffer (50 mM KH_2PO_4 and 50 mM K_2HPO_4 buffer, pH = 6.0) containing 0.5% hexadecyl trimethylammonium bromide detergent (0.5 mL buffer/sample). Following thorough vortexing, homogenates were centrifuged at 20,000 g at 4°C for 10 min, and aliquots of the supernatant were put in Eppendorf tubes. MPO activity was assayed using 3,3`5,5`-tetramethyl-benzidine-H_2O_2, and the reactions were carried out in 96-well microplates at room temperature. The absorbance at 450 nm was measured using a microplate reader. MPO activities were normalised to total protein content as measured by the Lowry method [70].

VI. Western blot

The GPX4 protein expression was measured from pancreatic tissue homogenates using Western blot analysis. Sonication was used to homogenise pancreatic tissue on ice in a buffer containing: 10 mM Na-HEPES, 1 µM $MgCl_2$, 10 mM KCl, 1 mM DL-dithiothreitol, 5 mM iodoacetamide, 4 mM benzamidine-HCl, 1 mM phenylmethyl sulfonylfluoride. Sample protein concentration was determined using the Bradford protein assay, followed by denaturation through boiling in sodium dodecyl sulfate (SDS)-Laemmli Sample buffer for 10 min. The samples were separated using SDS polyacrylamide gel (15 %) electrophoresis, and 64 µg of protein was loaded per lane. The gels were stained with Coomassie brilliant blue (to confirm equal loading of proteins for Western blot analysis) or transferred to a nitrocellulose membrane for 1 h at 100 V. The nitrocellulose membranes were blocked in Pierce™ Clear Milk Blocking Buffer (Thermo Fisher Scientific, Waltham, MA, USA) overnight at 4 °C before incubating with rabbit anti-GPX4 (cat.no.: MA5-32827) antibody at 1:10,000 dilution for 1 h at room temperature. Glyceraldehyde-3-phosphate dehydrogenase (GAPDH; cat.no.: PA1-987) was used (at 1:5000) as a loading control. The immunoreactive protein was visualised by enhanced chemiluminescence, using horseradish peroxidase-conjugated anti-rabbit immunoglobulin (cat.no.: 31460) at 1:10,000 dilution. Quantitative analysis of the results was achieved using the ImageJ software (NIH, Bethesda, MD, USA). The blot images were cropped, and only the relevant bands are shown in the figures.

VII. mRNA extraction and reverse transcription

Following the transfer of a small piece of the pancreas to 1 mL of TRI-reagent, the samples were homogenised using an IKA Ultra Turrax (Type: TP18/10; Janke and Kunkel IKA, Staufen im Breisgau, Germany) and the homogenates were stored at −80°C until use (for a maximum of 1 or 2 days). Total RNA isolation was performed utilising chloroform/isopropanol extraction. Briefly, phase separation was accomplished by adding 200 µL of chloroform to the samples, shaking vigorously for 15 min, allowing them to stand, and then centrifuging at 12,000 g for 15 min at 4°C. The top aqueous phase was aspirated into an empty Eppendorf tube from the resulting three phases, and 500 µL of isopropanol was added. After vortexing, the samples were allowed to stand for a few minutes and centrifuged at 12,000 g for 10 min at 4°C. The supernatant was removed, and the formed RNA precipitate was washed with 1 mL of 75 % ethanol. Following centrifugation (7,500 g for 5 min at 4°C), the supernatant was removed again, and the RNA was redissolved in 70 µL of RNAse-free water. After quantifying and assessing purity using a NanoDrop instrument (Thermo Fisher Scientific, Waltham, MA, USA), RNA integrity was determined by agarose gel electrophoresis. Two micrograms of total RNA were used for reverse transcription to cDNA. The PCR protocol for reverse transcription was started at 25°C for 10 min, followed by 37°C for 2 h, 85°C for 5 min, then 4°C. cDNA was stored at −20°C until further use.

VIII. Quantitative real-time PCR

Quantitative real-time PCR reactions were carried out using the Luminaris Colour HiGreen qPCR Master Mix (Thermo Fisher Scientific, Waltham, MA, USA) with specific primers (listed in Table 2). The total reaction mix volume was 10 µL. The reaction mixture components were the following: cDNA sample, 0.4 µM forward and reverse primer, Luminaris Colour HiGreen qPCR Master Mix and nuclease-free water. The thermal cycling protocol for the quantitative real-time PCR was set according to the manufacturer's instructions. All primers used in relative gene expression measurements were verified with the Oligoanalyzer program from Integrated DNA Technologies (Coralville, IA, USA; https://www.idtdna.com/pages/tools/oligoanalyzer). Gradient PCR was performed to determine the appropriate annealing temperature of the primers. The housekeeping gene in mRNA studies was *Gapdh*.

Table 2. Oligonucleotide primer pairs used for the determination of relative gene expression

Gene	5′−3′ primer pairs	Product (bp)
Cth	F: TTTGAATACAGCCGCTCTGGA R: GAAGTACCTGTTGGTGCCTCC	192
Cbs	F: TTGCGGTACTGGTCTAGGATG R: TCATCGTGATGCCAGAGAAG	178
Hmox1	F: CACAGGGTGACAGAAGAGGCTAA R: CTGGTCTTTGTGTTCCTCTGTCAG	96
Sod1	F: ATTACAGGATTAACTGAAGG R: CAATGATGGAATGCTCTC	238
Sod2	F: CAGACCTGCCTTACGACTATGG R: CTCGGTGGCGTTGAGATTGTT	113
Cat	F: TCAGGTGCGGACATTCTA R: ATTGCGTTCTTAGGCTTCT	204
Fth1	F: GCAGGATATAAAGAAACCAGACCG R: TGTCAGTAGCCAGTTTGTGC	125
Txnrd1	F: CAGCCCTGAAGCCGAACAA R: TGTGGATTGAGCAGTCACCC	869
Gapdh	F: GACAACTTTGGCATCGTGGA R: ATGCAGGGATGATGTTCTGG	133

IX. Pancreatic acinar cell isolation

Mouse pancreatic acinar cells were isolated according to Williams et al., with collagenase digestion [71]. Briefly, after the animals were sacrificed, the pancreas was removed, washed, and placed into ice-cold PS. The tissue was then cleaned of fat and lymph nodes on ice. The Digest solution utilised in the following steps contained the following in DMEM/F12: 2 mM L-glutamine, 0.25 mg/mL soybean trypsin inhibitor (Thermo Fisher Scientific, Waltham, MA, USA), 2.5 mg/mL bovine serum albumin and 4,500 U/g pancreas type 4 collagenase (Worthington Biochemical Co., Lakewood, USA). Following cleaning, the pancreas was cut into small pieces in 5 mL Digest solution. The tissue was incubated for 10 min in a shaking water bath (150 rpm) at 37°C. Then, the digestion medium was replaced with fresh medium, and the tissue was incubated for an additional 50 min with shaking. After digestion, the acinar cells were washed twice by centrifugation at 4°C, 50 g for 2 min, then resuspended in acinar cell culture medium, which contained the following in DMEM without phenol red: 2 mM L-glutamine, 0.25 mg/mL soybean trypsin inhibitor. The weight of the cellular supernatant was quantified by an analytical scale, and the final cell suspension was set to 15 mg cells/mL. The

cells were placed in a 37°C CO_2 incubator. The viability of the acini was rapidly determined using the trypan blue technique, and they were used for *in vitro* measurements if their viability was greater than 90 %.

X. Acinar viability measurements

3-(4,5-dimethylthiazol-2-yl)-2,5-diphenyltetrazolium bromide (MTT), Calcein-AM, and propidium iodide (PI) methods were employed to determine cellular viability. Actively respiring cells convert MTT via mitochondrial reductases, thereby reflecting cellular metabolic activity. Calcein-AM is retained by viable cells with intact membranes and indicates intracellular esterase activity, whereas PI indicates cellular necrosis. Isolated pancreatic acinar cells were seeded on 8-well microscope slides and treated with the following treatment solutions or with a specific combination of them: 30 µM ATB-346; 240 µM DMTS; 100 µM DATS; 10 µM GYY4137; 0.3 µM AP39; 0.17 mg/ml Poly80 with 0.4 % DMSO (vehicle control); 90 mg/ml Poly80 (vehicle control); 0.5 µM 1S,3R-RSL 3 (RSL 3); 5 µM erastin, 1 µM CCT137690 (CCT); 0.5 µM staurosporine (MedChemExpress; Monmouth Junction; NJ; USA); 1 nM Cer; 50 mM EtOH with 20 µM POA; 500 µM hydrogen peroxide (H_2O_2); 50 µM menadione; 60 mM L-arginine-HCl (L-arg); 0.1, 0.3, and 0.5 mM sodium chenodeoxycholate (CDC); or 1 % Triton X-100. All treatment solutions were prepared in acinar cell culture medium.

For the MTT assay, acinar cells were treated for 5 h at 37°C. Then, 0.5 mg/mL MTT was administered to the cells, and they were incubated for an additional 3 h with the dye and the treatments. After 8 h (5 and 3 h incubations), the formed formazan crystals were dissolved in DMSO, and the absorbances were measured by a microplate reader using a 595 nm filter. The Triton X-100 treatment served as the negative control, while untreated cells were the positive controls (considered 100 % viable).

For the Calcein-AM and PI assays, 1 µM Calcein-AM, 0.7 µg/ml PI, and 1.25 µg/ml H33342 were applied to the cells 30 min before the end of the treatment times, where Calcein-AM stained only viable cells with intact membranes, PI stained the nuclei of cells with compromised membranes, and H33342 stained all the cell nuclei. At the end of the treatment times, images of pancreatic acinar cells were captured (4 images / well) by an Axio Observer 7 (Carl Zeiss, Oberkochen, Germany) fluorescent microscope with Zen 2.6 Pro software. The following excitation/emission wavelengths were utilised: 495/515 for Calcein-AM; 533 – 558/570 – 645 for PI; 365/420 – 470 for H33342. ImageJ software was used to measure the areas of Calcein-AM, PI, and H33342 stainings. The percent of metabolic activity was

calculated by dividing the areas of Calcein-AM and H33342. Cellular necrosis was quantified by calculating the area of PI divided by the area of H33342. Triton X-100 treatment was considered to result in 100% toxicity.

XI. Measurement of reactive oxygen species

The intracellular ROS was determined by a microfluorescence method. Pancreatic acinar cells were seeded into a 96-well plate and exposed to the following treatment solutions either individually or in combination, all prepared in acinar cell culture medium: 30 μM ATB-346; 240 μM DMTS; 0.17 mg/ml Poly80 with 0.4% DMSO; 0.5 μM RSL 3; 5 μM erastin, 1 μM CCT; 1 nM Cer; 50 mM EtOH with 20 μM POA; 10, 30, and 50 μM menadione; 60 mM L-arg; 0.5 mM CDC.10 μM 6-carboxy-2',7'-dichlorodihydrofluorescein diacetate (carboxy-H2DCFDA), and 1.25 μg/ml H33342 were applied to the cells 30 min before the end of the 8 h treatment. Following the 8 h treatment, the 96-well plate was placed into a FLUOstar OPTIMA plate reader, and every 4 min a measurement was performed for 3 h, utilising 490/544 (carboxy-H2DCFDA) and 390/445 – 455 (H33342) excitation/emission wavelengths. ROS was quantified by dividing the carboxy-H2DCFDA and H33342 fluorescence intensities at 2 h.

XII. Real-time measurement of intracellular Ca^{2+} concentration

The intracellular Ca^{2+} concentration (ic[Ca^{2+}]) was monitored in real time using an Axio Observer 7 fluorescent microscope. Acinar cells were seeded in standard HEPES solution and loaded with 5 μM FURA-2-AM (Biotium, Fremont, CA, USA) for 30 – 90 min in a humidified atmosphere at 37°C containing 5 % CO_2. Then, the cells were placed on a poly-L-lysine-coated (5 μL, 0.01 % w/v) coverslip and incubated for 20 min to allow attachment to the surface. During the measurement, cells were perfused with the following solutions in the indicated order: (1) standard HEPES solution; (2) DMTS (0 or 240 μM); (3) 0.1 nM Cer or 1 nM Cer with or without 240 μM DMTS; (4) DMTS (0 or 240 μM); (5) standard HEPES solution; (6) 100 μM carbachol. The perfusion rate was 4 – 6 mL/min, and five to fifteen small areas (regions of interest) of 3 – 10 cells were monitored. 340 and 380 nm excitation wavelengths were utilised, and the 340/380 fluorescence excitation ratio was measured at 510 nm. One ic[Ca^{2+}] measurement was obtained per second. For the quantitative assessment of Ca^{2+} responses, the number (shown as frequency) and height (shown as calcium response) of individual spikes recorded between 480 and 960 s (8 min) were counted and averaged to be presented as mean ± standard deviation (SD). In case of supramaximal (1 nM) Cer administration, the area under the curve and the decreasing slope of ic[Ca^{2+}] response were calculated.

XIII. LC-MS/MS measurement of low molecular weight metabolites from pancreatic tissue and serum samples

Measurements were based on the method published by Akaike et al [72]. The following low-molecular-weight metabolites were determined: cysteine, cysteine persulfide, glutathione, glutathione persulfide, and sulfide. Briefly, frozen pancreatic tissue was homogenised with a dismembrator, then resuspended in ice-cold methanol containing 5 mM β-(4-hydroxyphenyl)ethyl iodoacetamide (HPE-IAM). After sonication, the derivatisation was performed at 37ºC for 20 min, followed by centrifugation (14000 g; 10 min; 4ºC). Then, 100 µl of the supernatant was acidified with 10 % formic acid (FA) and diluted two-fold with 0.1 % FA/H_2O before injection. Tissue pellets were dissolved in 1 % SDS in phosphate-buffered saline, and following sonication, protein content was measured using a BCA assay (Pierce BCA Protein Assay Kit, Thermo Fisher Scientific, Waltham, MA, USA).

75 µl of ice-cold methanol containing 5 mM HPE-IAM was added to 25 µl of the serum sample. Then the mixtures were incubated at 37ºC for 20 min and centrifuged at 14000 g, for 10 min, at 4ºC. The supernatant was acidified with 10 % FA and diluted two-fold with 0.1 % FA/H_2O before injection.

Liquid chromatography-tandem mass spectrometry (LC-MS/MS) measurements were carried out on a Thermo Q-Exactive Focus Orbitrap mass spectrometer coupled to a Thermo Vanquish UHPLC (ultra-high-performance liquid chromatograph), and the samples were analysed with two different methods. MS/MS detection was conducted in positive ionisation mode, and higher-energy collisional dissociation was used to detect the analytes.

Measurement of derivatised analytes was conducted on a Phenomenex Kinetex C18 (50 × 2.1 mm, 2.6 µm) column with eluents 0.1 % FA/H_2O (A) and 0.1% FA/MeOH (B). The initial 5 % B was linearly increased first to 13 % in 2 min, then to 95 % in 4 min, held there for 0.5 min, then lowered back to 5 % B in 0.1 min and held there for 3.4 min before the next injection. The flow rate was 0.5 ml/min, and the column was thermostated at 40°C.

XIV. Measurement of MDA

The level of MDA, an indicator of oxygen radical-induced lipid peroxidation, was measured in tissue samples using a commercial MDA Colourimetric Assay Kit, as described by the manufacturer.

XV. Statistical analysis

The sample size calculation was performed prior to *in vivo* studies with G ∗ Power (effect size: 1.8; power: 0.95; alpha error probe: 0.05). Values represent means with SD. Experiments were evaluated by one- or two-way ANOVA followed by Dunnett's or Tukey's *post-hoc* test (GraphPad Prism, GraphPad Software LLC, version 10.5.0). Normality was verified utilising visual assessment (Q-Q plot) and statistical testing (Shapiro-Wilk test). The Brown-Forsythe test was used to assess the homogeneity of variances. If necessary, the Kruskal-Wallis test was performed, followed by Dunn's *post-hoc* test. $P < 0.05$ was accepted as statistically significant.

RESULTS

I. Comparison of organosulfurs against experimental AP

I.1. Organosulfur molecules dose-dependently ameliorate the severity of Cer-induced AP in mice

Three different doses of each organosulfur molecule (ATB-346, DMTS, DATS, GYY4137, AP39) were employed to assess their effects on Cer-induced AP in FVB/N mice. The pancreata of the control group exhibited normal morphology (Fig. 2A). AP induced by supramaximal doses of Cer resulted in increased pancreatic water content, intensive leukocyte infiltration, MPO activity, serum amylase activity, and 40–50% tissue damage (Figs. 2-4). The administration of 2 × 20 μmol/kg ATB-346 did not affect the severity of the disease. In contrast, the 2 × 40 μmol/kg ATB-346 treatment significantly reduced the histological (oedema, leukocyte infiltration, cellular damage) parameters (Figs. 2B-D), and the highest dose of ATB-346 (2 × 80 μmol/kg) markedly decreased both histological and laboratory (water content, MPO, serum amylase) parameters as well (Figs. 2B-G).

Similar results were observed when investigating the effects of various doses of DMTS and DATS in the same Cer-induced AP model (Fig. 3). Representative histological sections demonstrated that AP caused damage to the pancreatic tissue, while both DMTS and DATS were able to ameliorate this damage in a dose-dependent manner (Figs. 3A, G). DMTS treatments at doses of 2 × 400 and 2 × 600 μmol/kg proved ineffective, whereas the administration of DMTS at 2 × 800 μmol/kg significantly reduced the severity of AP (Figs. 3B-F). Administering 2 × 25 μmol/kg DATS did not impact the severity of the disease. However, both 2 × 50 and 2 × 100 μmol/kg DATS treatments significantly reduced the degree of AP-induced increases in pancreatic oedema, leukocyte infiltration, cellular injury, and water content (Figs. 3H-K). Only the highest dose of DATS (2 × 100 μmol/kg) could decrease tissue MPO and serum amylase activities (Figs. 3L-M).

To examine the effects of GYY4137 and AP39 on pancreatic injury, varying doses were administered in Cer-induced AP (Fig. 4). Histological sections revealed severe tissue damage characterised by oedema, inflammatory cell infiltration, and acinar cell necrosis during the disease course (Figs. 4A, H). The lowest dose of GYY4137 (2 × 25 μmol/kg) significantly reduced the tissue damage but did not affect other measured parameters during AP. Administering GYY4137 at a 2 × 50 μmol/kg dose lowered the Cer-induced cellular damage and serum amylase activity (Figs. 4D, G). However, the treatment with 2 × 100 μmol/kg

GYY4137 significantly reduced all measured values, thereby alleviating the severity of AP (Figs. 4B-G). AP39 at a 2 × 0.25 µmol/kg dose significantly reduced both oedema and tissue damage, as well as serum amylase activity (Figs. 4I, K, N), while the lowest AP39 dose (2 × 0.125 µmol/kg) was ineffective. Treatment with the highest dose of AP39 (2 × 0.5 µmol/kg) markedly decreased all the AP severity parameters (Figs. 4I-N).

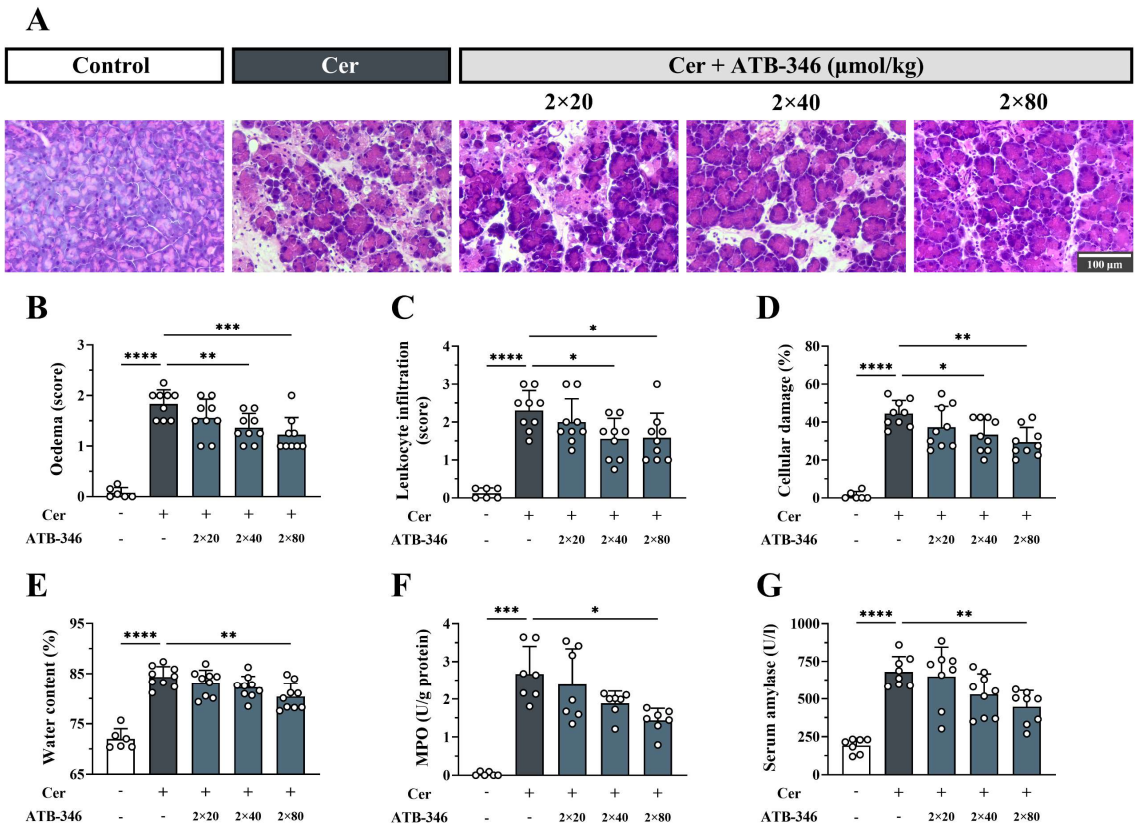

FIG 2. The effect of ATB-346 on the severity of cerulein (Cer)-induced necrotising acute pancreatitis (AP). Mice were treated *per os* with 2 × 20, 2 × 40 or 2 × 80 µmol/kg ATB-346, whereas intraperitoneal injection with 10 × 50 µg/kg Cer was used to induce AP. Control animals received physiological saline instead of Cer, or vehicle instead of ATB-346. The animals were sacrificed 12 h after the first Cer or physiological saline injection. (A) Representative histopathological images of pancreatic tissues of the treatment groups. Bar charts demonstrate the extent of pancreatic (B) oedema (evaluation of histological sections), (C) leukocyte infiltration, (D) cellular damage, (E) water content (as measured by the dry-wet weight ratio), (F) myeloperoxidase (MPO) activity, and (G) serum amylase activity. Values represent means with standard deviation (SD). (B–G) One-way ANOVA was carried out, followed by Dunnett's post-hoc test, where all of the groups were compared to the Cer-only group, *p < 0.05; **p < 0.01; ***p < 0.001; ****p < 0.0001.

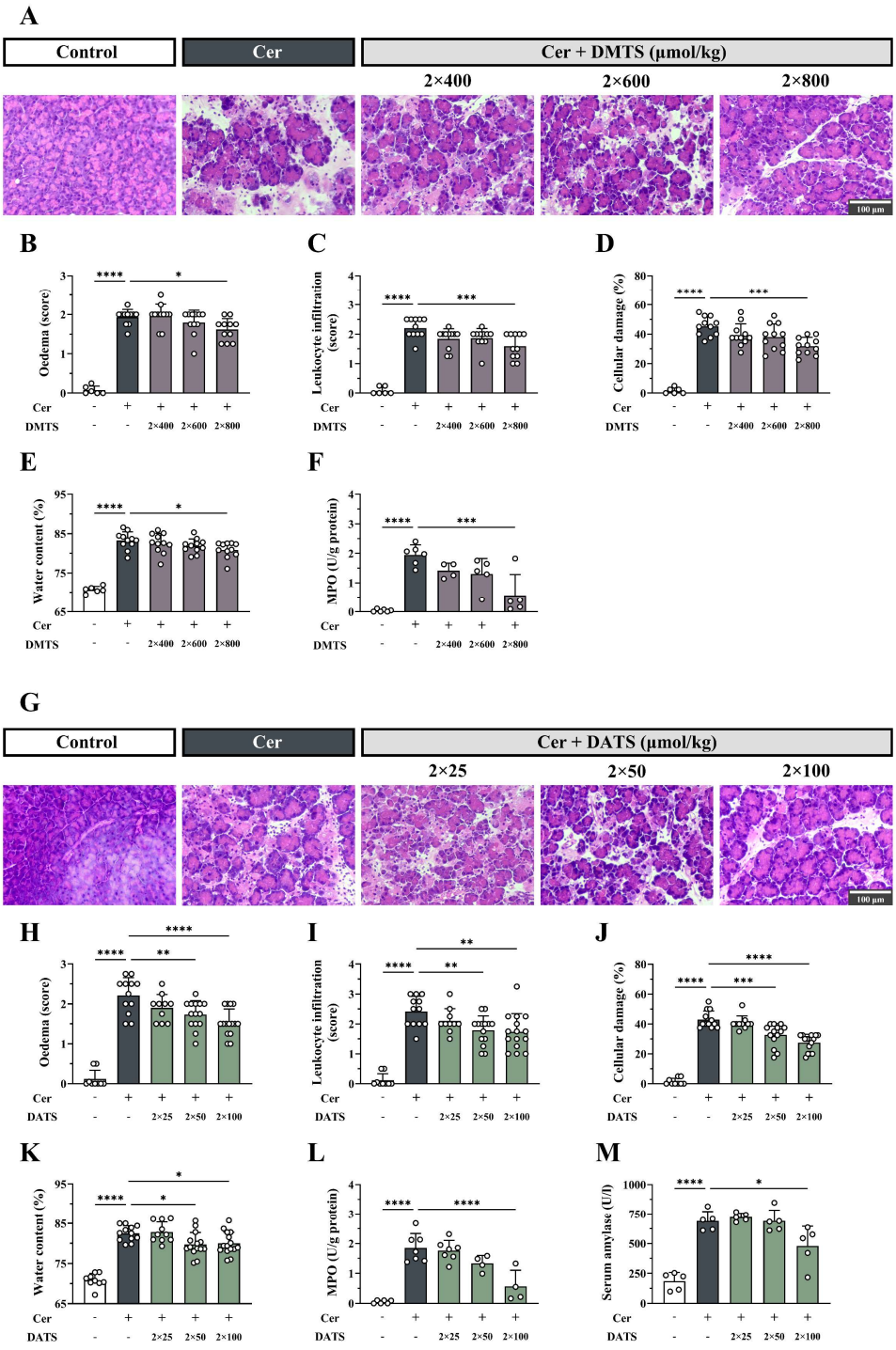

FIG 3. The effects of dimethyl trisulfide (DMTS) and diallyl trisulfide (DATS) on the severity of Cer-induced necrotising AP. Mice were treated subcutaneously with 2 × 400, 2 × 600 or 2 × 800 μmol/kg DMTS or intraperitoneally with 2 × 25, 2 × 50 or 2 × 100 μmol/kg DATS, whereas intraperitoneal injection with 10 × 50 μg/kg Cer was used to induce AP. Control animals received physiological saline rather than Cer, or vehicle instead of DMTS or DATS. The animals were sacrificed 12 h after the first Cer or physiological saline injection. (A, G) Representative histopathological images of pancreatic tissues of the treatment groups. Bar charts demonstrate the extent of pancreatic (B, H) oedema (evaluation of histological sections), (C, I) leukocyte infiltration, (D, J) cellular damage, (E, K) water content (as measured by the dry-wet weight ratio), (F, L) MPO activity, and (M) serum amylase activity. Values represent means with standard deviation (SD). (B–F, H–M) One-way ANOVA was carried out, followed by Dunnett's post-hoc test, where all of the groups were compared to the Cer-only group, *$p < 0.05$; **$p < 0.01$; ***$p < 0.001$; ****$p < 0.0001$.

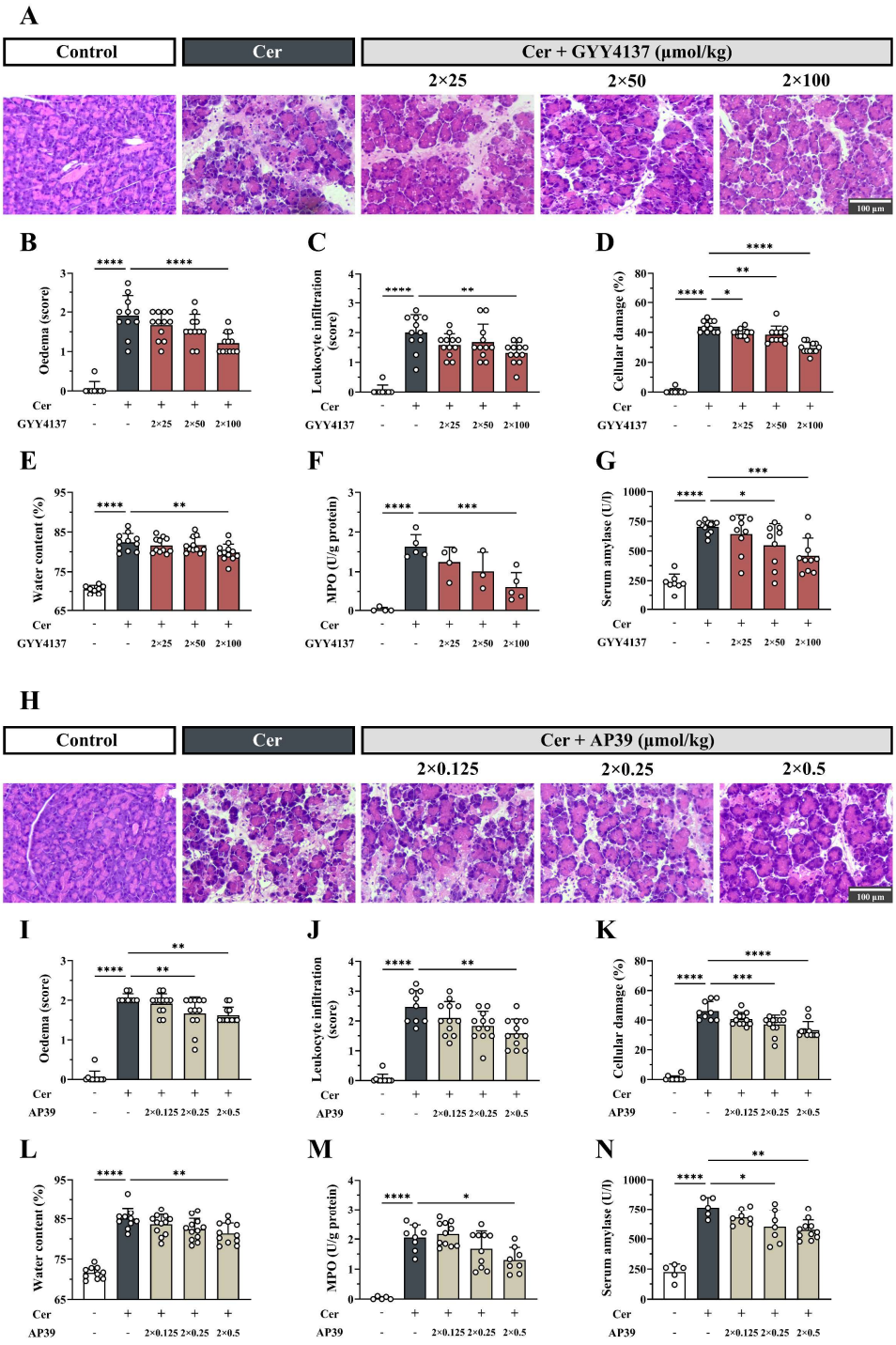

FIG 4. The effects of GYY4137 and AP39 on the severity of Cer-induced necrotising AP. Mice were treated intraperitoneally with 2 × 25, 2 × 50 or 2 × 100 μmol/kg GYY4137 or with 2 × 0.125, 2 × 0.25 or 2 × 0.5 μmol/kg AP39, whereas intraperitoneal injection with 10 × 50 μg/kg Cer was used to induce AP. Control animals received physiological saline instead of Cer, or vehicle instead of GYY4137 or AP39. The animals were sacrificed 12 h after the first Cer or physiological saline injection. (A, H) Representative histopathological images of pancreatic tissues of the treatment groups. Bar charts demonstrate the extent of pancreatic (B, I) oedema (evaluation of histological sections), (C, J) leukocyte infiltration, (D, K) cellular damage, (E, L) water content (as measured by the dry-wet weight ratio), (F, M) myeloperoxidase (MPO), and (G, N) serum amylase activities. Values represent means with standard deviation (SD). (B–G, I–N) One-way ANOVA was carried out, followed by Dunnett's post-hoc test, where all of the groups were compared to the Cer-only group, *$p < 0.05$; **$p < 0.01$; ***$p < 0.001$; ****$p < 0.0001$.

I.2. *In vitro* protective effects of organosulfur molecules against AP-inducing agents

To investigate the cytoprotective properties of these organosulfur molecules, cellular viability studies were conducted using the MTT and PI assays. The following organosulfur concentrations could be safely administered and were selected for further experiments: 240 μM DMTS; 100 μM DATS; 10 μM GYY4137; 0.3 μM AP39; 30 μM ATB-346. To investigate the cytoprotective effects of organosulfur molecules, primary pancreatic acinar cells were treated with AP-inducing agents, namely Cer, L-arg, and CDC (Fig. 5). The administration of 60 mM L-arg and 0.5 mM CDC significantly lowered the acinar metabolic activity (Fig. 5A-B) and caused toxic effects at 8 h (Figs. 5C-D). In contrast, 240 μM DMTS, 0.3 μM AP39, and 30 μM ATB-346 effectively restored the metabolic activity compared to the L-arg-only group, whereas only 240 μM DMTS could mitigate the adverse effect of CDC (Fig. 5A-B). All applied organosulfur treatments markedly decreased the L-arg- and CDC-induced toxicity (Figs. 5C-D). Administration of 1 nM Cer caused 16.9 ± 4.2 % toxicity at 8 h, which was significantly reduced by all organosulfur treatments, suggesting cytoprotective effects (Fig. 5E). In case of Cer administration, metabolic activity was not assessed, as Cer alone markedly alters the metabolic activity and can lead to false positive results.

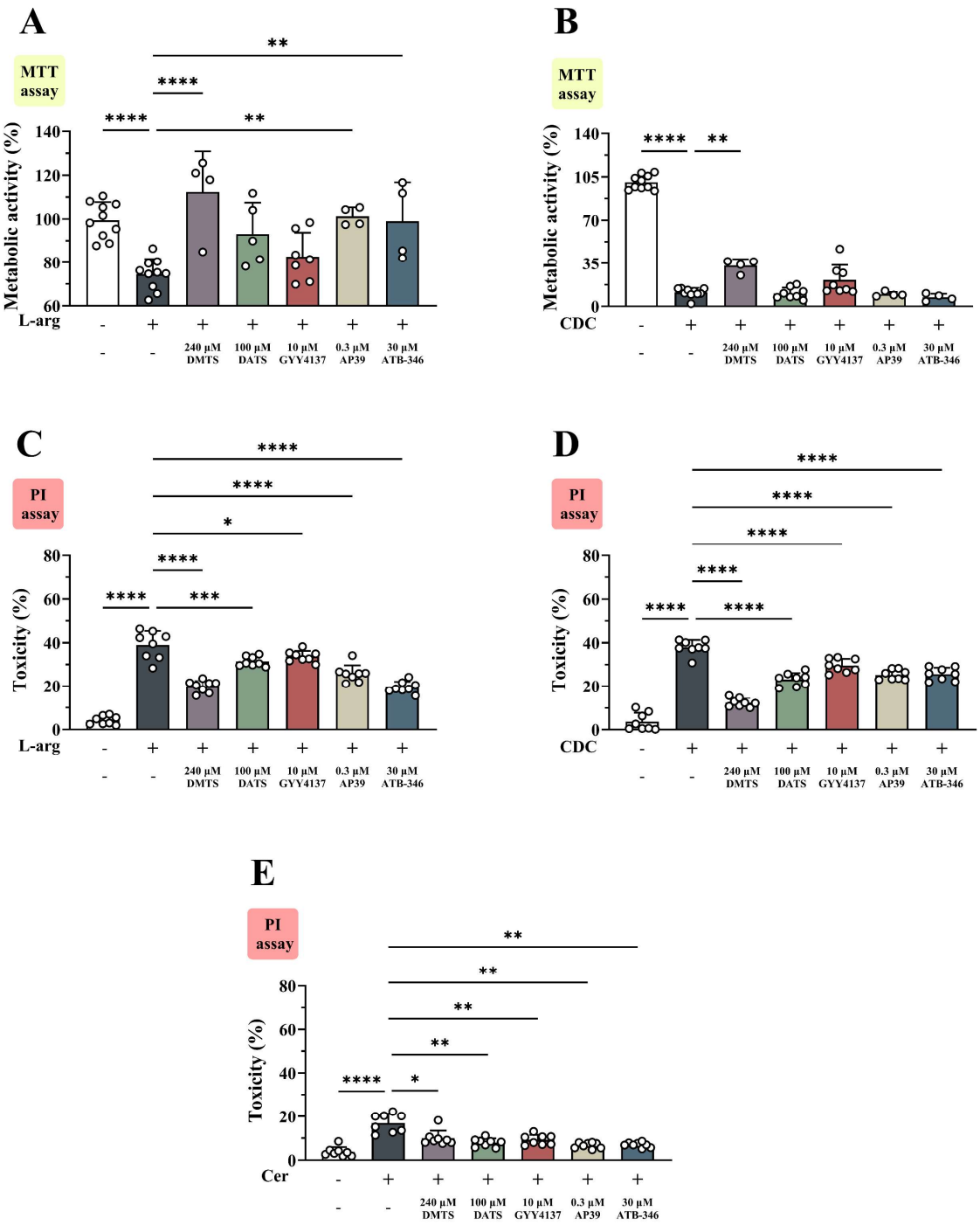

FIG 5. Metabolic activity and toxicity measurements on isolated pancreatic acinar cells. The effects of 60 mM L-arginine-HCl (L-arg), 0.5 mM sodium chenodeoxycholate (CDC), or 1 nM cerulein (Cer) and their combination with each organosulfur molecule (240 µM DMTS, 100 µM DATS, 10 µM GYY4137, 0.3 µM AP39, 30 µM ATB-346) on isolated mouse acinar cells were measured by (A-B) 3-(4,5-dimethylthiazol-2-yl)-2,5-diphenyltetrazolium bromide (MTT) and (C-E) propidium iodide (PI) methods. Both the MTT (metabolic activity) and the PI (toxicity) methods were used after 8 h of treatment. Values represent means with standard deviation (SD). One-way ANOVA was carried out, followed by Dunnett's post-hoc test, *$p < 0.05$; **$p < 0.01$; ***$p < 0.001$; ****$p < 0.0001$.

II. The anti-inflammatory effect of DMTS in experimental AP

II.1. DMTS reduces the severity of AP in mice when administered with AP induction

Among the five organosulfur molecules, DMTS and ATB-346 were further investigated. An alternative model of necrotising AP induced by EtOH-POA treatment was also employed in FVB/N mice (Fig. 6). The treatment doses of DMTS (3 × 600 and 3 × 800 μmol/kg) were given at 1, 6, and 12 h following the onset of the inflammation. The EtOH-POA AP model significantly increased the pancreatic oedema and leukocyte infiltration (Fig. 6A-C). The administration of DMTS did not affect the pancreatic water content and oedema during AP (Fig. 6B); however, it markedly reduced the leukocyte infiltration and MPO activity at both doses (Fig. 6C-D). Cellular damage was detected in the EtOH-POA AP model, reaching ~35 % (Fig. 6E). DMTS treatments with 3 × 600 and 3 × 800 μmol/kg doses significantly reduced the cellular damage.

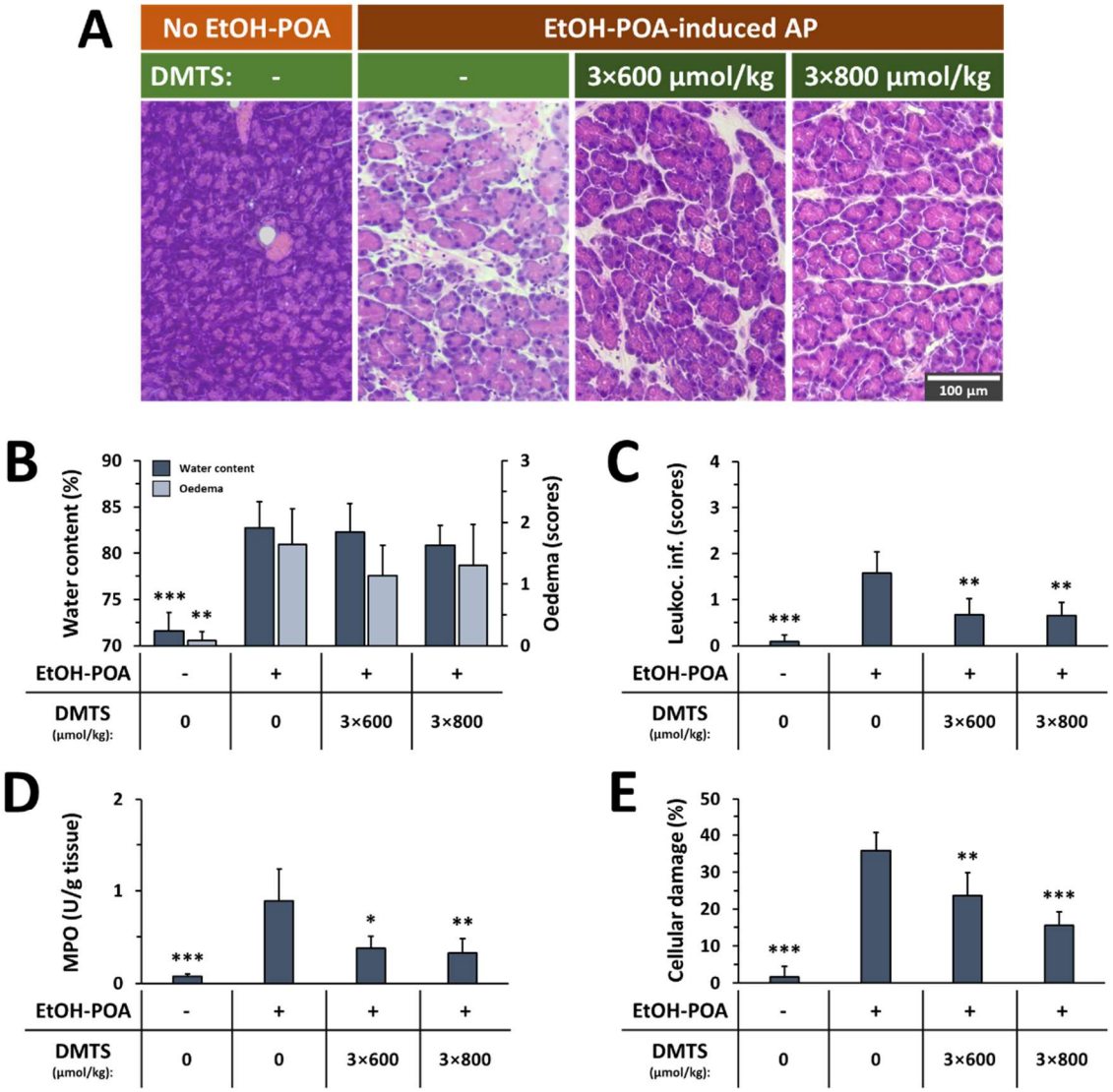

FIG 6. DMTS administration reduces the severity of ethanol and palmitoleic acid (EtOH-POA)-induced necrotising AP. Mice were treated subcutaneously with 3 × 600 or 3 × 800 µmol/kg DMTS, whereas intraperitoneal injection with 2 × 1.35 g/kg EtOH and 2 × 150 mg/kg POA was used to induce AP. Control animals received physiological saline instead of EtOH-POA or vehicle instead of DMTS. The animals were sacrificed 24 h after the first EtOH-POA or physiological saline injection. (A) Representative histopathological images of pancreatic tissues of the treatment groups. Bar charts demonstrate the extent of pancreatic (B) water content (as measured by the dry-wet weight ratio) and oedema (evaluation of histological sections), (C) leukocyte infiltration, (D) MPO activity, and (E) cellular damage. Values represent means with standard deviation (SD). (B-E) One-way ANOVA was carried out, followed by Dunnett's post-hoc test, where all of the groups were compared to the Cer-only group, *p < 0.05; **p < 0.01; ***p < 0.001.

II.2. DMTS modulates physiological, but not pathophysiological intracellular Ca^{2+} signalling in acinar cells

The ic[Ca^{2+}] was monitored in real-time in isolated pancreatic acinar cells. To investigate the effect of Cer on ic[Ca^{2+}], cells were perfused with maximal (0.1 nM) and supramaximal (1 nM) concentrations of Cer (Fig. 7A-E). Application of 0.1 nM Cer resulted in global, oscillatory increases in ic[Ca^{2+}] (Fig. 7A). The Ca^{2+} stores were subsequently depleted, and a few minutes later, carbachol, an acetylcholine (ACh) receptor agonist, was unable to elicit a relevant Ca^{2+} signal. The DMTS pre-treatment had no effect on the Cer-evoked oscillation frequency (Fig. 7A-B), but there was a significant increase in the average height of Ca^{2+} signals when the Cer treatment was compared to the Cer + DMTS treatment (Fig. 7A, C). Additionally, in the Cer + DMTS group, a remarkable increase in ic[Ca^{2+}] could be registered in response to carbachol at the end of the experiment. The supramaximal concentration of Cer (1 nM) evoked an initial peak in the Ca^{2+} signal, followed by a return to the basal levels, and showed no further increase or oscillation during stimulation (Fig. 7D-G). The pre-treatment with DMTS did not affect the Cer-induced pathological Ca^{2+} signals.

II.3. DMTS reduces oxidative stress in mouse pancreatic acinar cells

Intracellular concentrations of ROS were measured using the general oxidative stress indicator carboxy-H2DCFDA after 8 h (Fig. 7H). Via a redox cycling mechanism, menadione promotes intracellular ROS production. All applied menadione concentrations (10, 30, 50 µM) markedly increased the intracellular ROS levels (Fig. 7H), whereas administering 240 µM DMTS significantly reduced the effect of menadione on ROS formation.

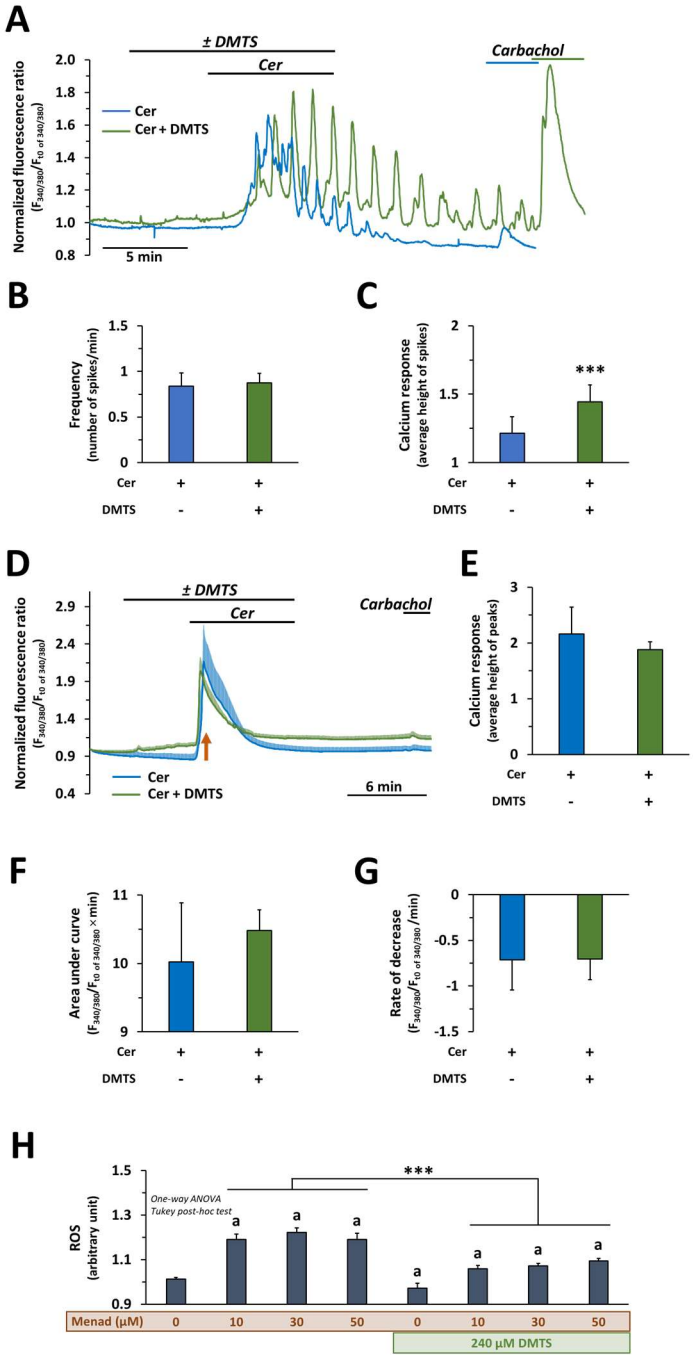

FIG 7. The effect of DMTS on intracellular Ca^{2+} signalling and its antioxidant property in mouse pancreatic acinar cells. (A) Representative trace of intracellular Ca^{2+} concentration (ic[Ca^{2+}]) in response to treatment with 0.1 nM cerulein (Cer) with or without 240 μM DMTS. At the end of the observation, acinar cells were subjected to 100 μM carbachol. The number (shown as frequency) and height (shown as calcium response) of individual spikes recorded between 480 and 960 s (8 min) were counted and plotted on panels B and C, respectively. (D-G) Treatment of cells with 1 nM Cer with or without 240 μM DMTS. At the end of the experiment, cells were subjected to 100 μM carbachol. When the ic[Ca^{2+}] reached the maximum (8 ± 0.5 min) the values were plotted on panel (E). The area under the curve was determined for the 1 nM Cer treatment (F), and the slope (decreasing part) of the response to Cer treatment (G). (H) Menadione (Menad) treatment at 10, 30, and 50 μM with or without 240 μM DMTS. Values represent means with standard deviation (SD). In the case of ic[Ca^{2+}], a total of 20 measurements were performed, and the cells were derived from 4 different animals. Statistics: (H) One-way ANOVA was performed, followed by Tukey's post-hoc test; and (B–C, E-G) Student's t-tests were applied. Statistically significant differences were marked in the following manner: ***$p < 0.001$; 'a', vs. control ($p < 0.05$).

II.4. DMTS increases serum sulfide and persulfide levels

To gain further insights into the protective effects of DMTS against AP, HPLC-MS/MS (high-performance liquid chromatography coupled with tandem mass spectrometry) based sulfur metabolome analyses were carried out. Mouse pancreatic tissue and serum samples were derived from the Cer-AP model (12 h sacrifice time) treated with 2 × 600 and 2 × 800 µmol/kg DMTS doses. DMTS treatments at doses of 2 × 600 and 2 × 800 µmol/kg increased the persulfide ratio (Cys-SSH/Cys-SH) in AP compared to the Cer-only group (Fig. 8A). Moreover, both 2 × 600 and 2 × 800 µmol/kg DMTS doses significantly increased the GSSH/GSH ratio (Fig. 8B). We also observed an elevated level of sulfide (H_2S) in the serum resulting from both DMTS doses in AP compared to the Cer-only group (Fig. 8C). In pancreatic tissue, the analyses revealed no significant differences in any of the measured metabolite levels between the Cer groups with or without DMTS treatment (Fig. 8D-F). Overall, our results showed that DMTS increases serum sulfide and low-molecular-weight persulfide levels and counteracts the effect of Cer on GSH, but it did not alter the levels of any of the measured metabolites in pancreatic tissue.

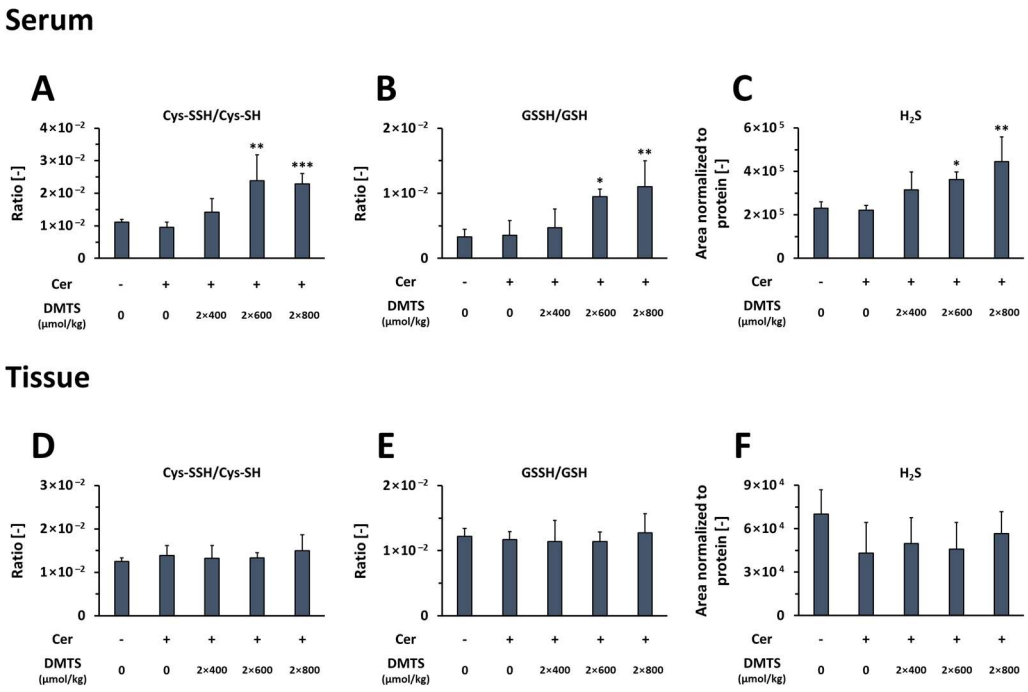

FIG 8. DMTS elevates serum sulfide and persulfide levels but does not affect pancreatic persulfidation and sulfide. The bar charts show cysteine (Cys-SH) and glutathione (GSH) persulfidation levels in serum (A–B) and pancreatic tissue samples (D–E), respectively. Sulfur metabolome analyses of sulfide (H_2S) levels in serum (C) and tissue samples (F). Values represent means with standard deviation (SD). (B, D–F) One-way ANOVA was performed, followed by Dunnett's post-hoc test, where all of the groups were compared to the Cer-only group, *$p < 0.05$; **$p < 0.01$. (A, C) Kruskal-Wallis test was performed, followed by Dunn's post-hoc test, the groups were compared to the Cer-only group, *$p < 0.05$; **$p < 0.01$; ***$p < 0.001$. Abbreviations: Cys-SSH, cysteine persulfide; GSSH, glutathione persulfide.

III. The antioxidant and antiferroptotic actions of ATB-346 in experimental AP

III.1. ATB-346 reduces the severity of EtOH-POA-induced AP

To conduct a more thorough investigation of the impact of ATB-346 on pancreatic injury, it was employed to assess its effects on EtOH-POA-induced AP in FVB/N mice (Fig. 9). The treatment doses of ATB-346 (3 × 40 and 3 × 80 μmol/kg) were given at 2, 6, and 12 h following the onset of the inflammation. The EtOH-POA-induced AP elevated the extent of oedema, leukocyte infiltration, and pancreatic injury compared to the control group (Figs. 9A-E). Both doses of ATB-346 (3 × 40 and 3 × 80 μmol/kg) significantly reduced all histological parameters, while the highest dose of ATB-346 (3 × 80 μmol/kg) decreased the pancreatic water content during AP (Fig. 9E). The 3 × 40 and 3 × 80 μmol/kg ATB-346 doses also reduced tissue MPO and serum amylase activities compared to the AP-only group (Figs. 9F-G).

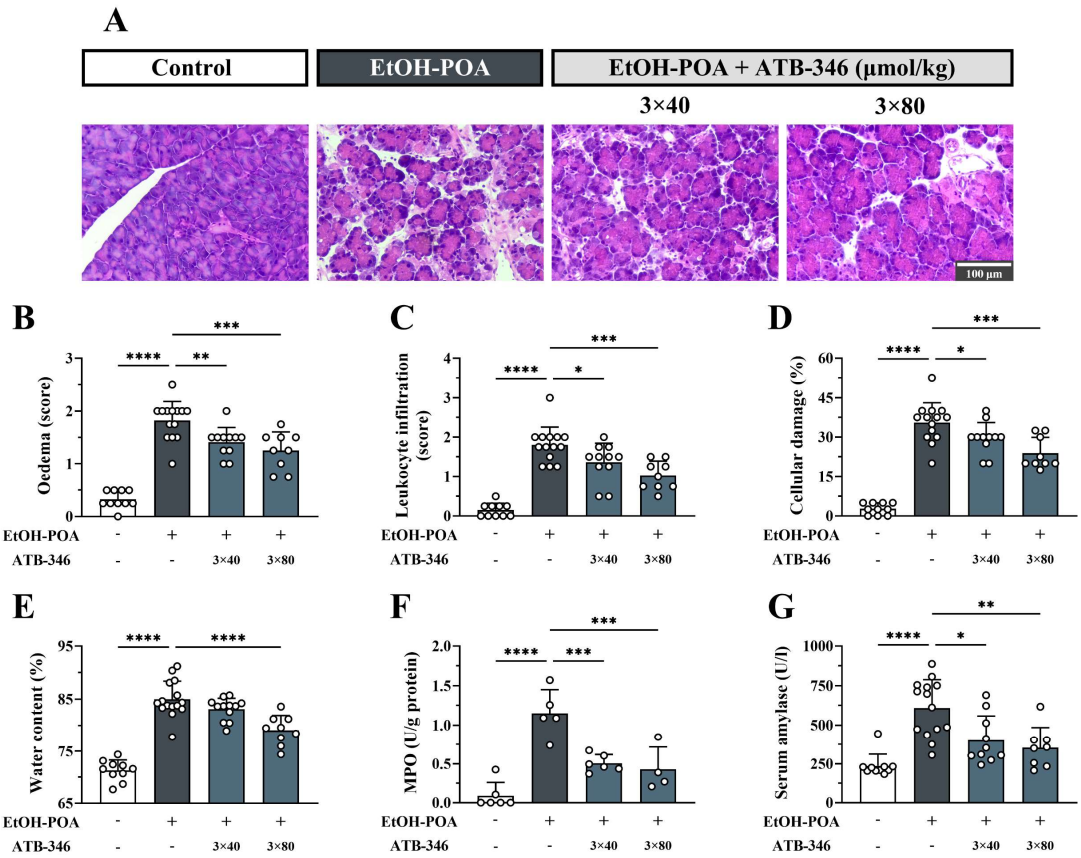

FIG 9. The effect of ATB-346 on the severity of EtOH-POA-induced necrotising AP. Mice were treated *per os* with 3 × 40 or 3 × 80 µmol/kg ATB-346, after AP was induced by intraperitoneal injection of 2 × 1.35 g/kg EtOH and 2 × 150 mg/kg POA. Control animals received physiological saline instead of EtOH-POA or vehicle instead of ATB-346. The animals were sacrificed 24 h after the first EtOH-POA or physiological saline injection. (A) Representative histopathological images of pancreatic tissues of the treatment groups. Bar charts demonstrate the extent of pancreatic (B) oedema (evaluation of histological sections), (C) leukocyte infiltration, (D) cellular damage, (E) water content (as measured by the dry-wet weight ratio), (F) myeloperoxidase (MPO) activity, and (G) serum amylase activity. Values represent means with standard deviation (SD). (B–G) One-way ANOVA was carried out, followed by Dunnett's post-hoc test, where all of the groups were compared to the EtOH-POA-only group, *$p < 0.05$; **$p < 0.01$; ***$p < 0.001$; ****$p < 0.0001$.

III.2. ATB-346 attenuates cellular oxidative stress and promotes cytoprotection

To investigate the antioxidant properties of ATB-346, the mRNA expression of genes involved in oxidative stress defence were determined. The relative gene expression of *Hmox1* mRNA markedly increased in both Cer- and EtOH-POA-induced AP (Fig. 10A). All tested ATB-346 doses (2 × 20, 2 × 40, and 2 × 80 μmol/kg) further elevated the *Hmox1* mRNA expression compared to the Cer-only group, whilst only the highest dose of ATB-346 (3 × 80 μmol/kg) increased the amount of *Hmox1* mRNA in the EtOH-POA AP model. The expression of the *Sod1* gene was significantly decreased in both employed AP models, and none of the ATB-346 treatments proved effective in restoring the mRNA of *Sod1* to control levels (Fig. 10B). A markedly reduced *Sod2* mRNA expression was also observed in Cer-induced AP, whereas in the EtOH-POA AP model, there was no significant change in the *Sod2* mRNA compared to the control group (Fig. 10C). In both AP models, the highest doses of ATB-346 (2 × 80 μmol/kg and 3 × 80 μmol/kg) significantly increased the expression of *Sod2* mRNA. The relative gene expression of *Cat* mRNA decreased in both Cer- and EtOH-POA-induced AP. Treatments with ATB-346 (3 × 40 and 3 × 80 μmol/kg) increased the amount of *Cat* mRNA solely in the EtOH-POA AP model (Fig. 10D).

Cellular viability measurements were also conducted to assess the protective effect of ATB-346 against oxidative stress-inducing agents using the Calcein-AM and PI methods (Figs. 10E-F). Treatment with 0.5 mM H_2O_2 significantly reduced acinar viability and evoked a toxic effect at 2 h (Fig. 10E). Conversely, 30 μM ATB-346 lowered the H_2O_2-induced toxicity, yet it was ineffective in increasing the cellular metabolic activity. Administering 50 μM menadione markedly decreased the acinar metabolic activity and resulted in 30 ± 6% toxicity at 2 h. In contrast, 30 μM ATB-346 effectively restored the metabolic activity compared to the menadione-only group (Fig. 10F).

Intracellular concentrations of ROS were measured using carboxy-H2DCFDA after 8 h. 1 nM Cer, 50 mM EtOH+POA, 60 mM L-arg, 0.5 mM CDC, and 50 μM menadione treatments all promoted intracellular ROS production, whereas 30 μM ATB-346 administration significantly reduced the effects of the aforementioned treatments on ROS formation (Figs. 10G-K). Administering 1 μM CCT resulted in no change in acinar ROS concentrations when compared to the control group (Fig. 10L). The treatment with 30 μM ATB-346 significantly decreased the intracellular ROS level, confirming its ability to scavenge ROS.

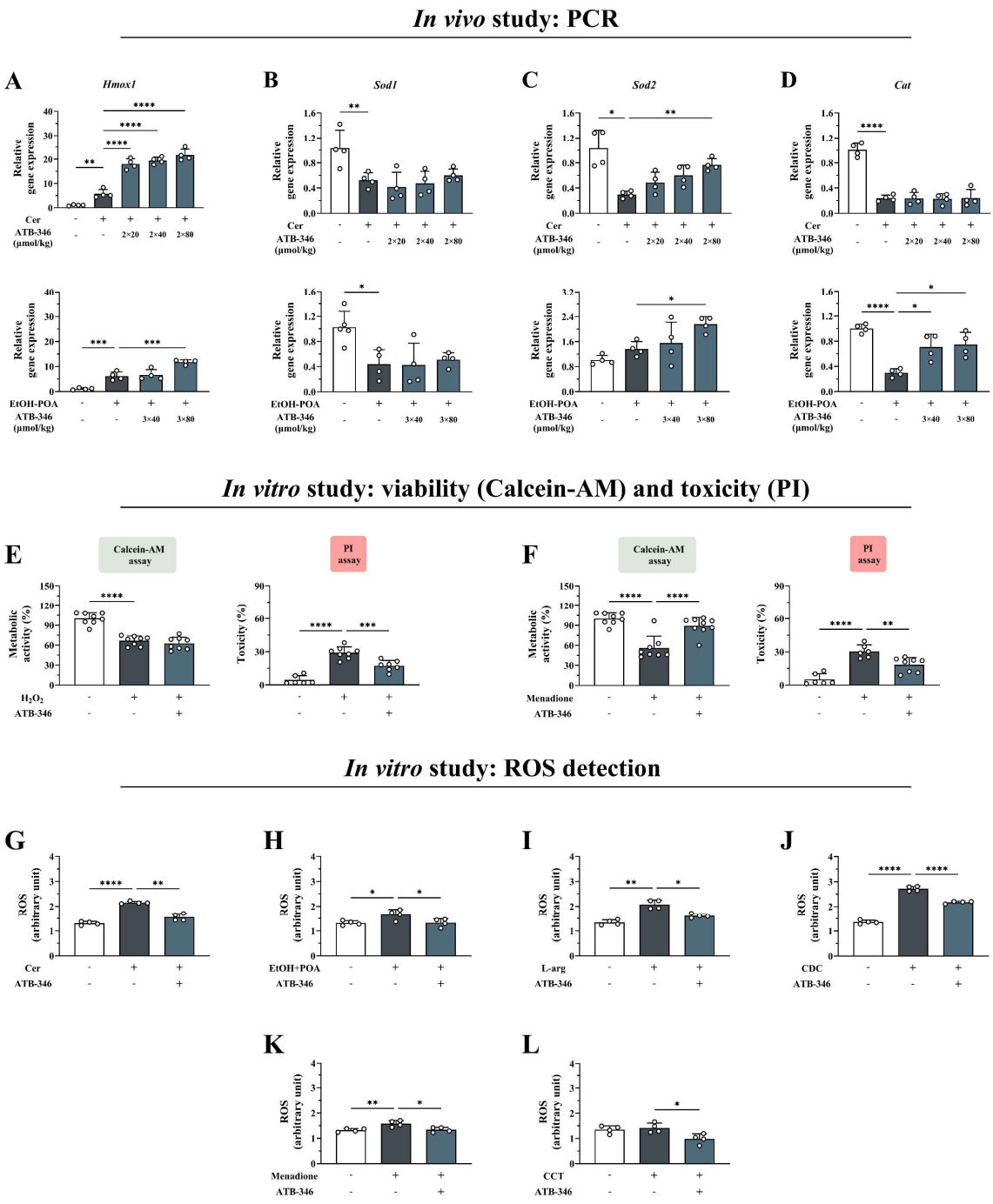

FIG 10. Assessment of the antioxidant properties of ATB-346. (A-D) The relative mRNA expression of genes involved in oxidative stress defence (*Hmox1*, *Sod1*, *Sod2*, *Cat)* was determined by qPCR in samples derived from *in vivo* experiments. (E-F) For *in vitro* acinar cell viability determination, both the Calcein-AM (indicated as metabolic activity) and the PI (indicated as toxicity) methods were used after 2 h of treatments. The effects of 0.5 mM H_2O_2, or 50 μM menadione and their combination with 30 μM ATB-346 on acinar cell viability were measured. (G-L) The general oxidative stress indicator 6-carboxy-2',7'-dichlorodihydrofluorescein diacetate (carboxy-H2DCFDA) was used on acinar cells to measure intracellular reactive oxygen species (ROS) production after 8 h of treatment. The following treatments and concentrations were utilised for the ROS method: 1 nM cerulein (Cer), 50 mM ethanol and 20 μM palmitoleic acid (EtOH+POA), 60 mM L-arginine-HCl (L-arg), 0.5 mM sodium chenodeoxycholate (CDC), 50 μM menadione, 1 μM CCT137690 (CCT). Values represent means with standard deviation (SD). (A-L) One-way ANOVA was carried out, followed by Dunnett's post-hoc test, *p < 0.05; **p < 0.01; ***p < 0.001; ****p < 0.0001.

Cth and *Cbs* are genes involved in the transsulfuration pathway and encode two of the three essential H_2S-producing enzymes. Both applied AP models decreased the expression of *Cth* and *Cbs* mRNA (Fig. 11A-B). In Cer-induced AP, the highest dose of ATB-346 (2 × 80 µmol/kg) markedly increased the relative expression of *Cbs* mRNA; however, it proved ineffective in all other instances.

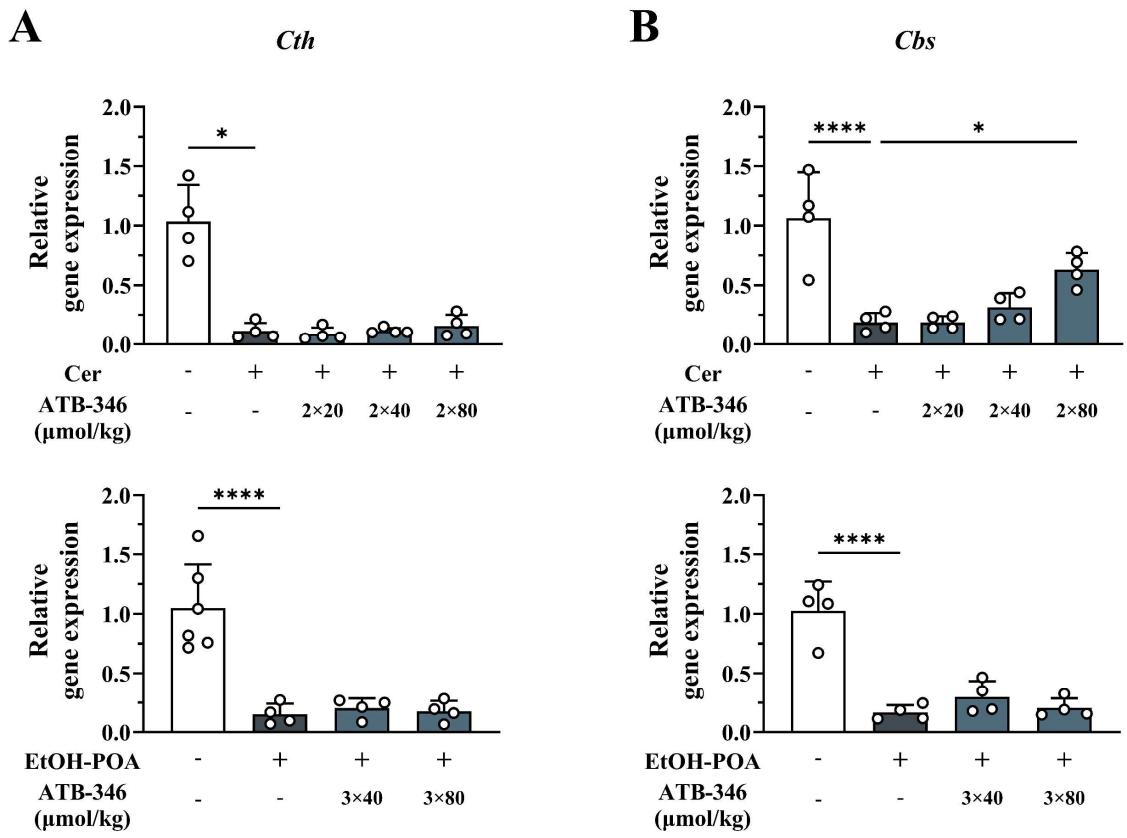

FIG 11. The effect of ATB-346 on enzymes responsible for endogenous H_2S production. The relative mRNA expression of genes involved in the transsulfuration pathway (*Cth*, *Cbs*) was determined by qPCR. Values represent means with standard deviation (SD). One-way ANOVA was carried out, followed by Dunnett's post-hoc test, *p < 0.05; ****p < 0.0001.

Antioxidant molecules can help combat oxidative stress and guard against lipid peroxidation, thereby offering protection against ferroptosis. Therefore, the effect of ATB-346 on ferroptosis was also investigated by measuring the mRNA expressions of *Fth1* and *Txnrd1*, the presence of MDA and GPX4, and the ability of ATB-346 to reduce the effects of ferroptosis-evoking agents (erastin, RSL-3). The relative expression of *Fth1* mRNA decreased in both Cer- and EtOH-POA-induced AP, whereas the highest doses of ATB-346 (2 × 80 μmol/kg and 3 × 80 μmol/kg) significantly increased the amount of *Fth1* mRNA (Fig. 12A). The mRNA expression of *Txnrd1*, an antioxidant gene, was markedly increased in the Cer AP model, whilst in EtOH-POA-induced AP, there was no significant change in the *Txnrd1* mRNA compared to the control group (Fig. 12B). ATB-346 treatments with 2 × 80 μmol/kg and 3 × 80 μmol/kg doses significantly increased the expression of *Txnrd1* mRNA. The increased expression of *Fth1* and *Txnrd1* mRNA following ATB-346 treatments indicates enhanced protection against ferroptosis.

MDA is a biomarker of oxidative stress and lipid peroxidation, and the detection of MDA can reflect the level of cellular damage from ferroptosis. Markedly elevated pancreatic MDA levels were observed in both Cer- and EtOH-POA-induced AP, and the highest doses of ATB-346 (2 × 80 μmol/kg and 3 × 80 μmol/kg) effectively reduced the MDA concentration (Fig. 12C). GPX4 is considered an essential regulatory factor in ferroptosis and a key target to counteract it. The protein expression of GPX4 was decreased in both employed AP models; however, the 2 × 80 μmol/kg and 3 × 80 μmol/kg ATB-346 doses significantly increased the GPX4 levels compared to the AP group (Fig. 12D).

Viability assays demonstrated that treatments with 5 μM erastin and 0.5 μM RSL 3, two ferroptosis inducers, significantly reduced the acinar metabolic activity and caused 54 ± 16 and 33 ± 11% toxicity at 8 h, respectively (Figs. 12E-F). Administering 30 μM ATB-346 restored the metabolic activity and significantly decreased the erastin- and RSL 3-induced toxicity. The 5 μM erastin and 0.5 μM RSL 3 treatments also increased the intracellular concentration of ROS, while 30 μM ATB-346 markedly reduced the ROS production caused by erastin or RSL 3 (Figs. 12G-H).

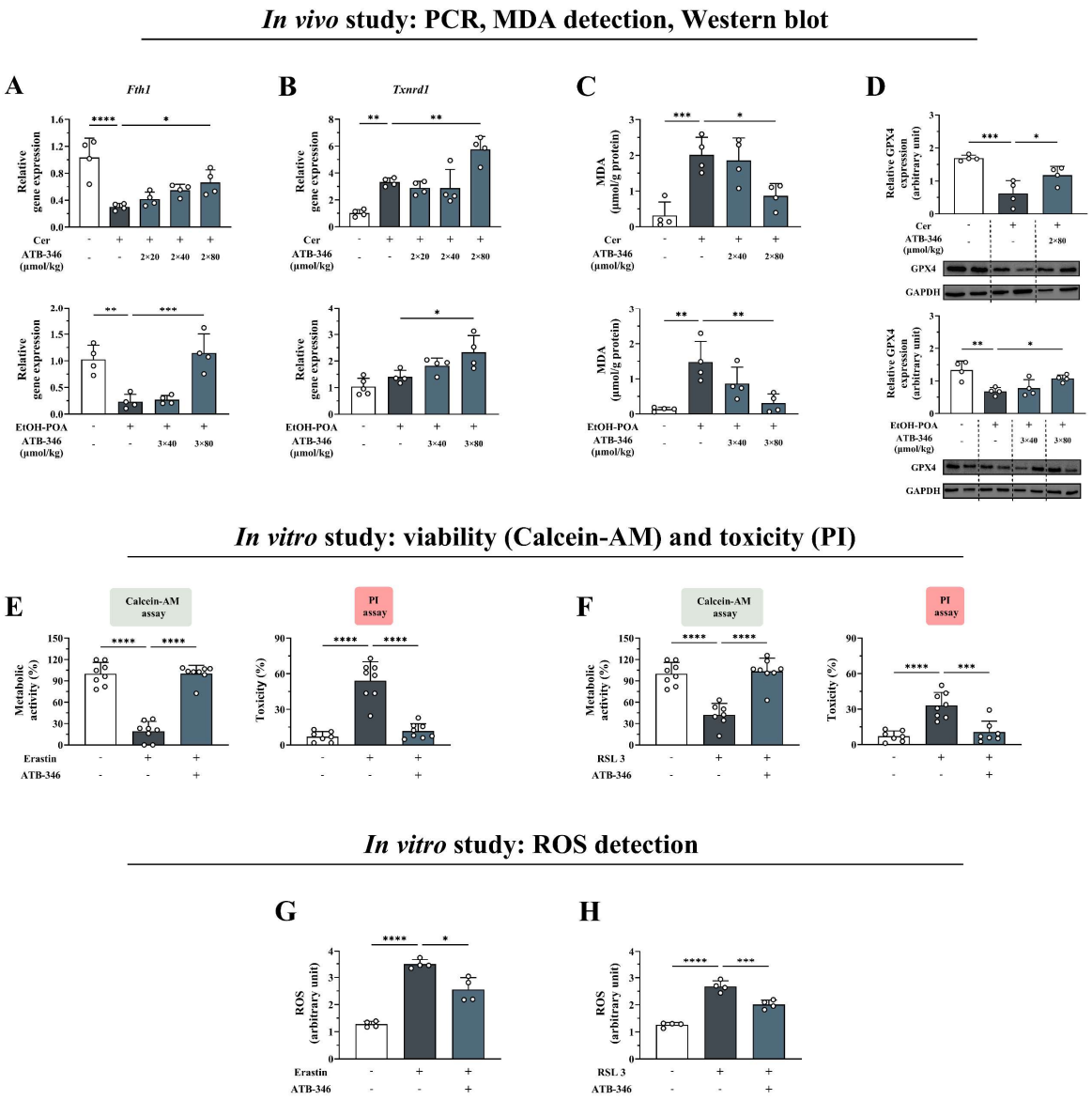

FIG 12. The effect of ATB-346 on ferroptosis. (A-B) The relative expression of ferroptosis-related genes (*Fth1*, *Txnrd1*) was determined by qPCR in samples derived from previously presented *in vivo* experiments. (C) Malondialdehyde (MDA), a biomarker of oxidative stress and lipid peroxidation, was measured in pancreatic tissue samples derived from *in vivo* experiments. (D) The representative Western blot images of pancreatic glutathione peroxidase 4 (GPX4) expression (samples derived from *in vivo* experiments) are depicted at the bottom, and the bar chart shows the densitometry of Western Blot images for pancreatic GPX4 level. Band intensities were assessed by using ImageJ software, and the GPX4 expression was normalised to glyceraldehyde-3-phosphate dehydrogenase (GAPDH) levels (E-F) For *in vitro* acinar cell viability determination, both the Calcein-AM (metabolic activity) and the PI (toxicity) methods were used after 8 h of treatment. The effect of 5 μM erastin, or 0.5 μM 1S,3R-RSL 3 (RSL 3) and their combination with 30 μM ATB-346 on acinar cell viability was measured. (G-H) The general oxidative stress indicator carboxy-H2DCFDA was used on acinar cells to measure intracellular ROS production after 8 h of treatment. The following treatments and concentrations were utilised for the ROS method: 5 μM erastin, 0.5 μM RSL 3. Values represent means with standard deviation (SD). (A–H) One-way ANOVA was carried out, followed by Dunnett's post-hoc test, *$p < 0.05$; **$p < 0.01$; ***$p < 0.001$; ****$p < 0.0001$.

DISCUSSION

I. Comparison of organosulfurs against experimental AP

AP remains a life-threatening inflammatory disease with no specific therapy, making it crucial to explore management options. Organosulfur compounds hold significant potential as drug candidates for various disease conditions, especially those linked to inflammation. In our study, treatments with all five organosulfur compounds (ATB-346, DMTS, DATS, GYY4137, and AP39) dose-dependently reduced the severity of Cer-AP by lowering both histological (oedema, leukocyte infiltration, cellular damage) and laboratory (water content, MPO, serum amylase) parameters. We also demonstrated that AP-inducing agents (L-arg, CDC, and Cer) caused cellular injury, and the administration of organosulfurs significantly reduced the resulting cytotoxic effects. All the organosulfur compounds we tested have been shown to exhibit cytoprotective effects, which can be attributed to various processes. These include the protection of protein function through protein persulfidation [73], the modulation of specific signalling pathways to mitigate the effects of oxidative stress, and the activation of the Kelch-like ECH-associated protein 1/Nrf2 system [74,75]. Based on the viability and toxicity measurements, GYY4137 and DATS exhibited less potent cytoprotection in comparison to ATB-346, DMTS, and AP39. Furthermore, we showed that ATB-346 and DMTS exert a more beneficial effect on disease severity relative to DATS, GYY4137 and AP39. Overall, DMTS and ATB-346 demonstrated the strongest cytoprotective effects and had similar impacts on the disease course. Our *in vivo* and *in vitro* results, along with the existing literature, confirm the anti-inflammatory potential of organosulfur compounds and suggest their suitability as drug candidates in AP.

II. The effect of DMTS on the severity of experimental AP

DMTS effectively safeguarded acinar cells and provided evidence of significant protection against experimental AP. To verify this anti-inflammatory effect, DMTS was employed in another AP model induced by EtOH-POA. DMTS administration decreased the pancreatic leukocyte infiltration, MPO activity, and cellular damage, thereby alleviating the severity of AP.

Intracellular Ca^{2+} signalling is a vital process that regulates cellular functions. However, pathophysiological events can cause abnormally elevated ic[Ca^{2+}], which in the case of acinar cells will initiate AP [76,77]. High but physiological concentration of Cer (0.1 nM) caused global ic[Ca^{2+}] oscillations, but these oscillations diminished within 5-7 min, and thereafter, the

ACh receptor agonist carbachol could not stimulate further Ca^{2+} release from the intracellular stores. Nevertheless, when the DMTS pre-treatment was applied, the 0.1 nM Cer-induced Ca^{2+} oscillations were sustained for longer periods, and carbachol could evoke a marked increase in ic[Ca^{2+}]. We assume that the intracellular Ca^{2+} stores become depleted in response to maximal Cer (0.1 nM) stimulation, and DMTS can prevent this. In addition, acinar cells become unresponsive to carbachol after maximal Cer administration, but their responsiveness was maintained in the presence of DMTS. However, the DMTS treatment did not affect the cellular ic[Ca^{2+}] response when the supramaximal and pathological Cer (1 nM) concentration was applied. Based on these observations, we can conclude that DMTS can moderate physiological, but not pathophysiological ic[Ca^{2+}].

Sulfur-donor molecules, such as polysulfides, are effective antioxidants, and this property may contribute to their beneficial effects in various diseases [78]. During AP, a significant amount of ROS is generated, and excessive ROS production and ATP depletion promote necrotic cell death rather than apoptosis [20]. Thus, we tested how DMTS protects primary acinar cells during oxidative stress. DMTS was protective when acinar cells were treated with the oxidative stress inducer, menadione, confirming its antioxidant capability. We hypothesised about the underlying mechanisms of this antioxidant effect. DMTS contains a sulfane sulfur (S^0), which makes it redox reactive [79]. Via transpersulfidation, DMTS can act as a sulfane sulfur donor, generating low-molecular-weight persulfides or persulfidate protein cysteine residues to conserve their activity by utilising the thioredoxin system [73]. Beyond its direct effect, DMTS, as a similar molecule to DATS, may also induce antioxidant enzymes via the Nrf2 pathway, but this warrants further investigation [80,81]. As mentioned earlier, excessive ROS production results in ATP depletion and necrosis. It would also be valuable in the future to examine intracellular ATP production during AP and DMTS treatment. Acinar necrosis, resulting from sustained ic[Ca^{2+}], loss of mitochondrial membrane potential, and oxidative stress, leads to the release of ATP, kallikrein, and trypsin into the extracellular space [14]. ATP and kallikrein will then activate macrophages and stellate cells, respectively, and elevate ic[Ca^{2+}] [82]. Thus, further studies aimed at elucidating how DMTS influences the disease pathophysiology should also investigate this aspect of the disease.

It has been proposed that H_2S signalling occurs via oxidative posttranslational modification of cysteine residues to persulfides [83–85]. Literature data indicate that, generally, in inflammatory diseases, H_2S production and increased persulfidation levels exert protective roles, but their synthesis is disrupted and decreased [86,87]. Interestingly, other studies focusing on AP reported opposite effects: experimental AP increased H_2S production, with enhanced

CBS and *CSE* expression [40]. Our sulfur metabolome analysis showed that, in experimental AP, the serum and pancreatic tissue levels of sulfide and protein persulfidations were unchanged. Here, we should note that the detection methods for sulfide and persulfidation significantly affect the outcomes and vary across papers, which could explain the diverse results [88]. Therefore, validated detection methods for sulfide and persulfidation are needed, and the result should not be overinterpreted [89,90]. In our experiments, DMTS increased the serum levels of sulfide and low-molecular-weight persulfides. This rise in persulfide levels may also suggest increased H_2S production. Our observations suggest that DMTS acts as an H_2S/S^0-donor, as evidenced by elevated serum H_2S levels and increased protein persulfidation, which might contribute to the observed protective effects against oxidative or inflammatory processes. It is also noteworthy that although H_2S may play a significant role in the potential mechanism of DMTS protecting against AP, it is currently very difficult to differentiate whether this effect is mediated by H_2S or persulfides/polysulfides. This is due to the fact that the currently available state-of-the-art detection protocols are limited and may artificially alter the speciation of these reactive sulfur compounds [89].

III. The effect of ATB-346 on the severity of experimental AP

NSAIDs, such as aspirin or naproxen, have anti-inflammatory, analgesic, and potential chemopreventive properties. ATB-346 is a naproxen derivative with a covalently attached H_2S donor moiety, which has shown its anti-inflammatory effect on various inflammatory diseases [44,65–67]. Taking into account the existing literature and our *in vivo* and *in vitro* results, ATB-346 was selected for further investigation. To confirm the potent anti-inflammatory effect of ATB-346 on AP severity, it was also utilised in a second necrotising AP model in mice induced by EtOH-POA. In line with the findings in Cer-AP, ATB-346 attenuated the severity of AP by decreasing all histological and laboratory parameters.

It is likely that the cytoprotective and anti-inflammatory properties of H_2S released from ATB-346 complement the anti-inflammatory effect of cyclooxygenase inhibition, resulting in the enhanced beneficial effects of ATB-346 compared to those of naproxen. Based on literature data, exogenous H_2S exerts its anti-inflammatory effect by activating the antioxidant Nrf2 [91], inhibiting the pro-inflammatory NF-κB [92], and suppressing the mitogen-activated protein kinase signalling pathways [93]. Given the H_2S-donor potential of ATB-346, the mRNA expression of genes involved in oxidative stress defence were determined in our study. The expression of *HMOX1*, *SOD1*, *SOD2*, and *CAT* reflects the antioxidant defensive ability of the pancreas [94–96]. ATB-346 treatments markedly increased the relative gene expression of

Hmox1, *Sod2*, and *Cat* in a dose-dependent manner, which may contribute to its protective effect. The activation of the transsulfuration pathway, induced by genes such as *CBS*, can attenuate oxidative stress by increasing cellular glutathione levels [97]. ATB-346 significantly elevated the relative expression of *Cbs* mRNA in Cer-AP, likely due to the exogenous H_2S release. Viability assays demonstrated that ATB-346 protects acinar cells against cytotoxicity caused by two commonly used oxidative stress inducers, H_2O_2 and menadione, confirming its antioxidant properties. During AP, in response to elevated ic[Ca^{2+}], acinar and inflammatory cells generate a significant amount of ROS [20]. The resulting oxidative stress and mitochondrial Ca^{2+} influx lead to a reduction in mitochondrial membrane potential and, consequently, to the inhibition of ATP production in acinar cells [14]. Therefore, we tested whether ATB-346 reduces intracellular ROS production and offers cytoprotection against both exogenous and endogenous ROS in primary acinar cells. AP-inducing agents (namely Cer, EtOH+POA, L-arg, and CDC) and menadione increased the intracellular ROS formation, whereas administering the necroptosis inducer aurora kinase inhibitor CCT resulted in no change in acinar ROS concentrations. ATB-346 markedly decreased the ROS production when used in combination with the aforementioned treatments, confirming that ATB-346 likely acts as a scavenger of ambient and induced ROS through H_2S release, thereby reducing oxidative damage.

Emerging research highlights the regulatory function of H_2S in lipid peroxidation and its complex interaction with lipid peroxides [34,39]. With growing experimental evidence that ferroptosis is involved in various diseases, including AP, its inhibition by antioxidants has become the focus of several studies [98,99]. As an antioxidant, ATB-346 may offer protection against ferroptosis by counteracting oxidative stress and preventing lipid peroxidation, possibly due to its H_2S-donor property and anti-inflammatory effects. Therefore, we investigated the impact of ATB-346 on the mRNA expression of genes involved in ferroptosis. *FTH1* plays a crucial role in maintaining cellular iron balance during ferroptosis and is involved in ferritinophagy, a selective form of autophagy [100]. The administration of ATB-346 significantly elevated the relative gene expression of *Fth1* mRNA, thereby likely limiting free iron and inhibiting the formation of lipid peroxides. *TXNRD1* maintains cellular redox balance by reducing thioredoxin and serves as a key regulator of various antioxidant pathways [101]. ATB-346 markedly increased the relative expression of *Txnrd1*, through which ATB-346 may reduce the accumulation of lipid peroxides. Lipid peroxidation products increase during ferroptosis, and catabolites such as MDA serve as valuable markers for oxidative stress [102]. MDA concentrations were markedly increased in both Cer- and EtOH-POA-induced AP, and

ATB-346 effectively decreased the MDA levels, indicating that ATB-346 mitigated the cellular damage caused by ferroptosis. GPX4 neutralises lipid peroxides and protects cells and membranes against peroxidation [103]. Wang et al. showed that exogenous H_2S released from NaHS activates the Nrf2/GPX4/GSH pathway and suppresses ferroptosis [104]. ATB-346 significantly increased the GPX4 protein expression, likely through the activation of the Nrf2 pathway triggered by the H_2S-releasing capacity of ATB-346. Inhibiting the GPX4/GSH antioxidant system with the ferroptosis inducer erastin (depleting GSH) or RSL 3 (inhibiting GPX4) led to cell death and increased intracellular ROS formation. ATB-346 administration effectively safeguarded acinar cells, indicating its capacity to support antioxidant defence by enhancing GSH levels and GPX4 activity, as well as independently of this pathway.

IV. Conclusion

This work provides evidence that all five tested organosulfur compounds exert anti-inflammatory and cytoprotective effects. Of the five, DMTS and ATB-346 provided significant protection against experimental AP and were selected for further investigation to gain insights into their mechanisms of action (Fig. 13). DMTS effectively alleviated the severity of two necrotising AP models, and we demonstrated that DMTS modulates physiological Ca^{2+} signalling, reduces ROS levels, and elevates serum sulfide and persulfide levels. These effects may result from its antioxidant properties, its role as an H_2S donor, and/or its ability to decrease leukocyte infiltration and inhibit MPO activity. ATB-346 attenuated the severity of two experimental AP models and demonstrated antioxidant properties by increasing the expression of antioxidant enzymes and reducing intracellular ROS concentrations. Additionally, it increased the expression of genes involved in ferroptosis, lowered MDA levels, and protected acinar cells from ferroptosis-inducing treatments. ATB-346 exerted this effect via the enhancement of the GPX4/GSH antioxidant system and also independently from it. The release of H_2S from ATB-346's donor moiety, combined with cyclooxygenase inhibition, may account for the aforementioned effects.

Our results demonstrate that organosulfurs have anti-inflammatory and cytoprotective effects, thus making them promising therapeutic agents in the treatment of AP. Overall, organosulfur compounds are worth further investigation in this potentially lethal disease.

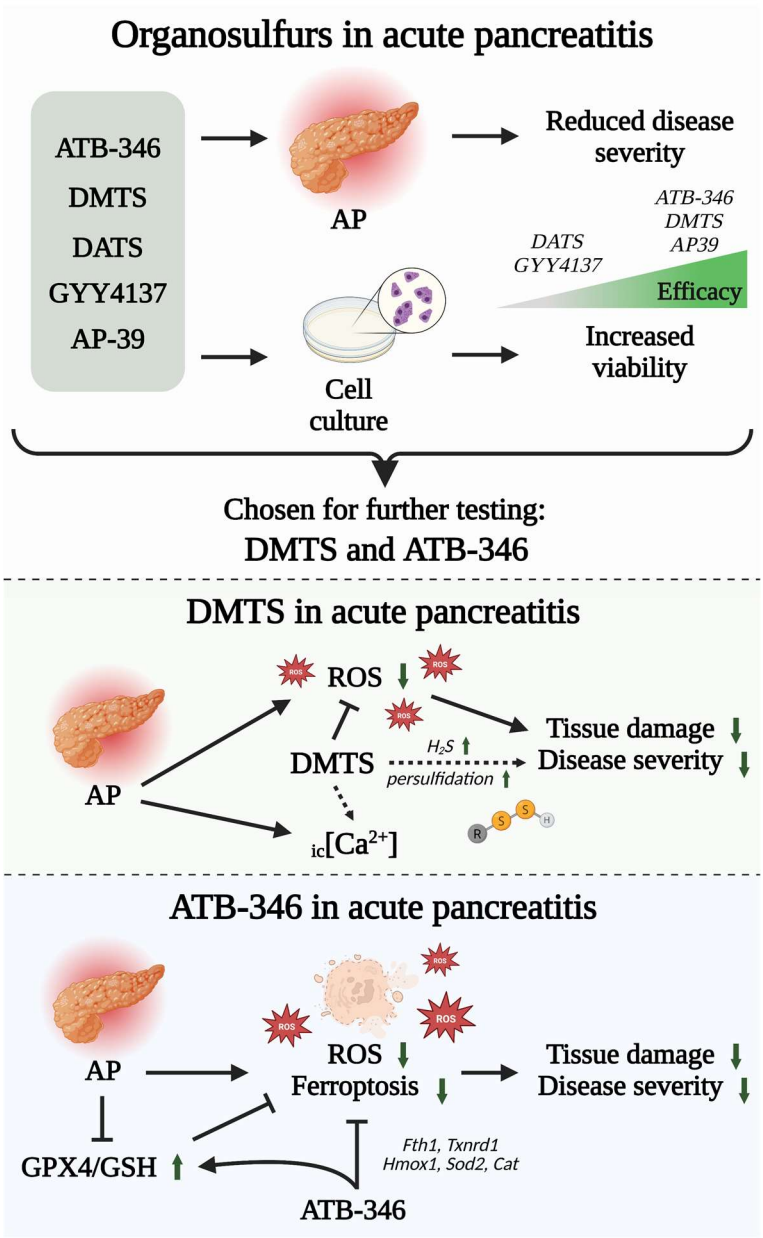

FIG 13. Summary of the effects of organosulfur compounds in experimental AP.

SUMMARIES

Summary of the thesis

Introduction: AP, an acute inflammatory disorder of the exocrine pancreas, is a potentially life-threatening disease with no specific treatment. Slow-releasing H_2S donor organosulfur compounds administered exogenously have been reported to exhibit anti-inflammatory and antioxidant effects across various disease conditions, but limited information exists regarding their impact on AP. Our objective was to comprehensively investigate and compare the five most widely studied organosulfurs (ATB-346, DMTS, DATS, GYY4137, AP39) as therapeutic agents against experimental AP in mice. Furthermore, we aimed to provide insights into the mechanisms of action of DMTS and ATB-346 in both *in vivo* and *in vitro* studies.

Methods: AP was induced in FVB/n mice either by hourly i.p. injections of Cer, or EtOH and POA. Different doses of organosulfur treatments were administered i.p., subcutaneously or *per os* simultaneously with AP induction. Disease severity was determined by evaluating pancreatic histological scoring, pancreatic water content, MPO and serum amylase activities. The relative mRNA expression of genes involved in oxidative stress defence (*Hmox1*, *Sod1*, *Sod2*, *Cat*), H_2S synthesis (*Cth*, *Cbs*), and ferroptosis (*Fth1*, *Txnrd1*) were determined by qPCR. Western blot experiments were performed to measure the pancreatic GPX4 protein expression. The level of MDA in pancreatic tissue samples was assessed by colourimetry. HPLC–MS/MS-based sulfur metabolome analyses were carried out to measure serum and tissue sulfide and persulfide levels. Mouse primary pancreatic acinar cells were isolated by collagenase digestion and used for *in vitro* assays (MTT, Calcein-AM, and PI) to determine cellular viability. Intracellular concentrations of ROS and ic[Ca^{2+}] were determined by microfluorimetry.

Results: Each organosulfur molecule (ATB-346, DMTS, DATS, GYY4137, AP39) dose-dependently decreased the histological and laboratory markers of inflammation in Cer-induced AP and demonstrated *in vitro* cytoprotective effects (MTT and PI assays). Additionally, DMTS and ATB-346 alleviated the severity of EtOH-POA-induced AP, confirming their potent anti-inflammatory effects. DMTS administration modulated physiological but not pathophysiological Ca^{2+} signalling and reduced the effect of menadione on intracellular ROS formation. Furthermore, it elevated serum H_2S levels and increased protein persulfidation. ATB-346 increased the mRNA expression of antioxidant (*Hmox1*, *Sod2*, *Fth1*, *Txnrd1*) genes, reduced the level of MDA, and enhanced the GPX4 protein expression. Ferroptosis- (erastin, RSL 3), oxidative stress- (H_2O_2, menadione), and AP-inducing (Cer, CDC, L-arg, EtOH-POA)

agents reduced the cellular metabolic activity (Calcein-AM assay) and induced acinar cell necrosis (PI assay). However, the administration of ATB-346 significantly decreased the toxic effects of the aforementioned substances. ATB-346 reduced ROS levels when isolated acinar cells were treated with menadione, ferroptosis- and AP-inducing agents.

Conclusions: This work provides evidence that all five tested organosulfur compounds exert anti-inflammatory and cytoprotective effects. Among the five organosulfurs, DMTS and ATB-346 exhibited the most potent cytoprotective effects and had similar impacts on the disease course. Our findings suggest that the beneficial effects of DMTS in AP could be due to its antioxidant properties and its role as an H_2S donor. We also revealed that the antioxidant and anti-inflammatory effects of ATB-346 are mediated through the enhancement of the GPX4 antioxidant system, as well as via GPX4-independent mechanisms. Our results indicate that organosulfurs possess anti-inflammatory and cytoprotective properties, thus making them promising candidates in the treatment of AP.

Summary of new findings

- All five organosulfurs (ATB-346, DMTS, DATS, GYY4137, AP39) reduced the severity of experimental AP and exerted cytoprotection
- DMTS and ATB-346 emerged as the most potent agents, and they were selected for further testing
- DMTS modulated physiological Ca^{2+} signalling and reduced the menadion-induced ROS levels
- DMTS increased serum H_2S levels and protein persulfidation, indicating H_2S donor properties
- ATB-346 upregulated pancreatic antioxidant genes (*Hmox1*, *Sod2*) and neutralised the produced ROS
- ATB-346 inhibited ferroptosis through the GPX4/GSH system, as well as by increasing the mRNA expression of *Fth1* and *Txnrd1*

FUNDING

This work was supported by EFOP-3.6.2–16–2017–00006, GINOP-2.3.2–15–2016–00034, NKFIH FK143566, NKFIH K135874, János Bólyai Research Grant (BO/00866/20/5).

ACKNOWLEDGEMENTS

First of all, I would like to express my most sincere thanks to my supervisor, **Dr. Lóránd Kiss**, and my mentor, **Prof. Dr. Zoltán Rakonczay**. I am grateful for their knowledge, guidance, and support; without it, this work would not have been possible.

I am also very grateful to our collaborating partners, **Prof. Dr. Erika Pintér**, **Prof. Dr. Péter Nagy**, **Prof. Dr. Péter Hegyi**, **Dr. József Maléth**, **Dr. Petra Pallagi**, **Dr. Viktória Venglovecz**, **Dr. Viktória Kormos**, **Dr. Gábor Pozsgai**, **Dr. Zoárd István Bátai**, **Dr. Ágnes Dombi**, **Dr. Ammar Al-Omari**, **Dr. Tamás Ditrói**, and **Eszter Petra Jurányi**, for their exceptional assistance and help in conducting certain experiments.

I would like to thank my colleagues, **Ágnes Dágó**, **Ola Salamah**, **Bálint Sándor**, **Dr. Gabriella Mihalekné Fűr**, **Dr. Emese Réka Bálint**, **Dr. Eszter Sára Kormányos**, **Beáta Adél Balog**, **Dr. Krisztina Csabafi**, **Dr. Júlia Szakács**, **Dr. Katalin Ibos**, **Dr. Sárközy Márta Julianna**, **Dr. Zsolt Bagosi**, **Dr. Zsolt Balla**, **Dr. Losonczi Réka**, **Dr. Kis Merse**, **Dr. Volford Dávid**, **Lilian Azar**, **Dr. Koncz István**, and **Dr. Miklós Jászberényi**, for their help, encouragement, and advice over the years. Special thanks to our team for filling the workplace with memorable moments.

This thesis could not have been realised without the valuable assistance and support of **Zsófia Bódai**, **Máté Márkus**, **Boglárka Takácsné Mihalik**, **Boglárka Gémes-Horváth**, **Tímea Börcsökné Püspök**, **Nóra Ildikó Vass**, **Gusztáv Kiss**, and **Zsuzsanna Fráter**.

Last, but not least, I owe special thanks to every member of my family and all my friends for their unwavering support, trust, and never-ending patience. I'm truly grateful to my parents, **István** and **Bernadett**, and my brother, **Máté**, for all the love and joyful moments they've shared with me. Special thanks to **Balázs** and **Nóra**, dear friends who have helped me immensely over the past few years. I am also grateful to **Zsófia** for all her advice, encouragement, and the countless joyful moments that have helped me during these last few difficult months. Their support inspires me every day, and I dedicate this thesis to them.

"Nothing in life is to be feared; it is only to be understood. Now is the time to understand more, so that we may fear less." — Marie Curie

REFERENCES

[1] Czakó L, Hegyi P, Rakonczay Z, Wittmann T, Otsuki M. Interactions between the endocrine and exocrine pancreas and their clinical relevance. Pancreatology 2009;9:351–9. https://doi.org/10.1159/000181169.

[2] Pallagi P, Hegyi P, Rakonczay Z. The Physiology and Pathophysiology of Pancreatic Ductal Secretion: The Background for Clinicians. Pancreas 2015;44:1211–33. https://doi.org/10.1097/MPA.0000000000000421.

[3] Hegyi P, Rakonczay Z. The role of pancreatic ducts in the pathogenesis of acute pancreatitis. Pancreatology 2015;15:S13-7. https://doi.org/10.1016/j.pan.2015.03.010.

[4] Peery AF, Crockett SD, Murphy CC, Lund JL, Dellon ES, Williams JL, et al. Burden and Cost of Gastrointestinal, Liver, and Pancreatic Diseases in the United States: Update 2018. Gastroenterology 2019;156:254-272.e11. https://doi.org/10.1053/j.gastro.2018.08.063.

[5] Garg PK, Singh VP. Organ Failure Due to Systemic Injury in Acute Pancreatitis. Gastroenterology 2019;156:2008–23. https://doi.org/10.1053/j.gastro.2018.12.041.

[6] Roberts SE, Morrison-Rees S, John A, Williams JG, Brown TH, Samuel DG. The incidence and aetiology of acute pancreatitis across Europe. Pancreatology 2017;17:155–65. https://doi.org/10.1016/j.pan.2017.01.005.

[7] Banks PA, Bollen TL, Dervenis C, Gooszen HG, Johnson CD, Sarr MG, et al. Classification of acute pancreatitis--2012: revision of the Atlanta classification and definitions by international consensus. Gut 2013;62:102–11. https://doi.org/10.1136/gutjnl-2012-302779.

[8] Olson E, Perelman A, Birk JW. Acute management of pancreatitis: the key to best outcomes. Postgrad Med J 2019;95:328–33. https://doi.org/10.1136/postgradmedj-2018-136034.

[9] Forsmark CE, Vege SS, Wilcox CM. Acute Pancreatitis. N Engl J Med 2016;375:1972–81. https://doi.org/10.1056/NEJMra1505202.

[10] Wang G-J, Gao C-F, Wei D, Wang C, Ding S-Q. Acute pancreatitis: etiology and common pathogenesis. World J Gastroenterol 2009;15:1427–30. https://doi.org/10.3748/wjg.15.1427.

[11] Yadav D, Whitcomb DC. The role of alcohol and smoking in pancreatitis. Nat Rev Gastroenterol Hepatol 2010;7:131–45. https://doi.org/10.1038/nrgastro.2010.6.

[12] Tsuang W, Navaneethan U, Ruiz L, Palascak JB, Gelrud A. Hypertriglyceridemic pancreatitis: presentation and management. Am J Gastroenterol 2009;104:984–91. https://doi.org/10.1038/ajg.2009.27.

[13] Barreto SG, Habtezion A, Gukovskaya A, Lugea A, Jeon C, Yadav D, et al. Critical thresholds: key to unlocking the door to the prevention and specific treatments for acute pancreatitis. Gut 2021;70:194–203. https://doi.org/10.1136/gutjnl-2020-322163.

[14] Petersen OH, Gerasimenko J V, Gerasimenko O V, Gryshchenko O, Peng S. The roles of calcium and ATP in the physiology and pathology of the exocrine pancreas. Physiol Rev 2021;101:1691–744. https://doi.org/10.1152/physrev.00003.2021.

[15] Saluja A, Dudeja V, Dawra R, Sah RP. Early Intra-Acinar Events in Pathogenesis of Pancreatitis. Gastroenterology 2019;156:1979–93. https://doi.org/10.1053/j.gastro.2019.01.268.

[16] Gukovskaya AS, Gukovsky I, Algül H, Habtezion A. Autophagy, Inflammation, and Immune Dysfunction in the Pathogenesis of Pancreatitis. Gastroenterology 2017;153:1212–26. https://doi.org/10.1053/j.gastro.2017.08.071.

[17] Sendler M, Dummer A, Weiss FU, Krüger B, Wartmann T, Scharffetter-Kochanek K, et al. Tumour necrosis factor α secretion induces protease activation and acinar cell necrosis in acute experimental pancreatitis in mice. Gut 2013;62:430–9. https://doi.org/10.1136/gutjnl-2011-300771.

[18] Gukovskaya AS, Vaquero E, Zaninovic V, Gorelick FS, Lusis AJ, Brennan M-L, et al. Neutrophils and NADPH oxidase mediate intrapancreatic trypsin activation in murine experimental acute pancreatitis. Gastroenterology 2002;122:974–84. https://doi.org/10.1053/gast.2002.32409.

[19] Karki R, Kanneganti T-D. The "cytokine storm": molecular mechanisms and therapeutic prospects. Trends Immunol 2021;42:681–705. https://doi.org/10.1016/j.it.2021.06.001.

[20] Armstrong JA, Cash NJ, Ouyang Y, Morton JC, Chvanov M, Latawiec D, et al. Oxidative stress alters mitochondrial bioenergetics and modifies pancreatic cell death independently of cyclophilin D, resulting in an apoptosis-to-necrosis shift. Journal of Biological Chemistry 2018;293:8032–47. https://doi.org/10.1074/jbc.RA118.003200.

[21] Liu X, Dou B, Zhu Q, Liu C. Targeting the programmed cell death signaling mechanism with natural products for the treatment of acute pancreatitis: a review. Front Pharmacol 2025;16. https://doi.org/10.3389/fphar.2025.1567552.

[22] Dixon SJ, Olzmann JA. The cell biology of ferroptosis. Nat Rev Mol Cell Biol 2024;25:424–42. https://doi.org/10.1038/s41580-024-00703-5.

[23] Yang WS, Kim KJ, Gaschler MM, Patel M, Shchepinov MS, Stockwell BR. Peroxidation of polyunsaturated fatty acids by lipoxygenases drives ferroptosis. Proc Natl Acad Sci U S A 2016;113:E4966-75. https://doi.org/10.1073/pnas.1603244113.

[24] Wang Y, Yan D, Liu J, Tang D, Chen X. Protein modification and degradation in ferroptosis. Redox Biol 2024;75:103259. https://doi.org/10.1016/j.redox.2024.103259.

[25] Chen X, Yu C, Kang R, Kroemer G, Tang D. Cellular degradation systems in ferroptosis. Cell Death Differ 2021;28:1135–48. https://doi.org/10.1038/s41418-020-00728-1.

[26] Ingold I, Berndt C, Schmitt S, Doll S, Poschmann G, Buday K, et al. Selenium Utilization by GPX4 Is Required to Prevent Hydroperoxide-Induced Ferroptosis. Cell 2018;172:409-422.e21. https://doi.org/10.1016/j.cell.2017.11.048.

[27] Fan R, Sui J, Dong X, Jing B, Gao Z. Wedelolactone alleviates acute pancreatitis and associated lung injury via GPX4 mediated suppression of pyroptosis and ferroptosis. Free Radic Biol Med 2021;173:29–40. https://doi.org/10.1016/j.freeradbiomed.2021.07.009.

[28] Liu K, Liu J, Zou B, Li C, Zeh HJ, Kang R, et al. Trypsin-Mediated Sensitization to Ferroptosis Increases the Severity of Pancreatitis in Mice. Cell Mol Gastroenterol Hepatol 2022;13:483–500. https://doi.org/10.1016/j.jcmgh.2021.09.008.

[29] Hou W, Xie Y, Song X, Sun X, Lotze MT, Zeh HJ, et al. Autophagy promotes ferroptosis by degradation of ferritin. Autophagy 2016;12:1425–8. https://doi.org/10.1080/15548627.2016.1187366.
[30] Chen Y, Yi X, Huo B, He Y, Guo X, Zhang Z, et al. BRD4770 functions as a novel ferroptosis inhibitor to protect against aortic dissection. Pharmacol Res 2022;177:106122. https://doi.org/10.1016/j.phrs.2022.106122.
[31] Sun Y, Chen P, Zhai B, Zhang M, Xiang Y, Fang J, et al. The emerging role of ferroptosis in inflammation. Biomed Pharmacother 2020;127:110108. https://doi.org/10.1016/j.biopha.2020.110108.
[32] Castro-Piedras I, Perez-Zoghbi JF. Hydrogen sulphide inhibits Ca2+ release through InsP3 receptors and relaxes airway smooth muscle. J Physiol 2013;591:5999–6015. https://doi.org/10.1113/jphysiol.2013.257790.
[33] Vandiver MS, Snyder SH. Hydrogen sulfide: a gasotransmitter of clinical relevance. J Mol Med 2012;90:255–63. https://doi.org/10.1007/s00109-012-0873-4.
[34] Munteanu C, Turnea MA, Rotariu M. Hydrogen Sulfide: An Emerging Regulator of Oxidative Stress and Cellular Homeostasis—A Comprehensive One-Year Review. Antioxidants 2023;12:1737. https://doi.org/10.3390/antiox12091737.
[35] Rodkin S, Nwosu C, Sannikov A, Raevskaya M, Tushev A, Vasilieva I, et al. The Role of Hydrogen Sulfide in Regulation of Cell Death following Neurotrauma and Related Neurodegenerative and Psychiatric Diseases. Int J Mol Sci 2023;24. https://doi.org/10.3390/ijms241310742.
[36] Zhu X-X, Zhao C-Y, Lu Q-B, Zhang A-Y, Meng X-Y, Su J-B, et al. Hydrogen sulfide as a new therapeutic target of pulmonary hypertension: an overview with update on immunomodulation. Front Pharmacol 2025;16. https://doi.org/10.3389/fphar.2025.1510275.
[37] Liu F, Li L, Yuan L, Yang J, Tang X, Liu J, et al. S-sulfhydration: Novel insights into the antioxidant and antiinflammation in age-related diseases. J Adv Res 2026;81:915–33. https://doi.org/10.1016/j.jare.2025.06.038.
[38] Layal H, Rajbongshi J, Kumar R, Pandey S, Mishra R, Yadav PK. Hydrogen sulfide in the brain as a silent neuroprotector in Alzheimer's disease. Neuroscience 2025;585:181–97. https://doi.org/10.1016/j.neuroscience.2025.08.057.
[39] Barayeu U, Schilling D, Eid M, Xavier da Silva TN, Schlicker L, Mitreska N, et al. Hydropersulfides inhibit lipid peroxidation and ferroptosis by scavenging radicals. Nat Chem Biol 2023;19:28–37. https://doi.org/10.1038/s41589-022-01145-w.
[40] Bhatia M, Gaddam RR. Hydrogen Sulfide in Inflammation: A Novel Mediator and Therapeutic Target. Antioxid Redox Signal 2021;34:1368–77. https://doi.org/10.1089/ars.2020.8211.
[41] Whiteman M, Li L, Rose P, Tan C-H, Parkinson DB, Moore PK. The Effect of Hydrogen Sulfide Donors on Lipopolysaccharide-Induced Formation of Inflammatory Mediators in Macrophages. Antioxid Redox Signal 2010;12:1147–54. https://doi.org/10.1089/ars.2009.2899.
[42] Dombi Á, Sánta C, Bátai IZ, Kormos V, Kecskés A, Tékus V, et al. Dimethyl Trisulfide

Diminishes Traumatic Neuropathic Pain Acting on TRPA1 Receptors in Mice. Int J Mol Sci 2021;22. https://doi.org/10.3390/ijms22073363.

[43] Wallace JL, Wang R. Hydrogen sulfide-based therapeutics: exploiting a unique but ubiquitous gasotransmitter. Nat Rev Drug Discov 2015;14:329–45. https://doi.org/10.1038/nrd4433.

[44] Van Dingenen J, Pieters L, Vral A, Lefebvre RA. The H2S-Releasing Naproxen Derivative ATB-346 and the Slow-Release H2S Donor GYY4137 Reduce Intestinal Inflammation and Restore Transit in Postoperative Ileus. Front Pharmacol 2019;10:116. https://doi.org/10.3389/fphar.2019.00116.

[45] Lee HH, Han MH, Hwang HJ, Kim G-Y, Moon S-K, Hyun J-W, et al. Diallyl trisulfide exerts anti-inflammatory effects in lipopolysaccharide-stimulated RAW 264.7 macrophages by suppressing the Toll-like receptor 4/nuclear factor-κB pathway. Int J Mol Med 2015;35:487–95. https://doi.org/10.3892/ijmm.2014.2036.

[46] Bhatia M, Sidhapuriwala JN, Sparatore A, Moore PK. TREATMENT WITH H2S-RELEASING DICLOFENAC PROTECTS MICE AGAINST ACUTE PANCREATITIS-ASSOCIATED LUNG INJURY. Shock 2008;29:84–8. https://doi.org/10.1097/shk.0b013e31806ec26.

[47] Dong Z, Shang H, Chen YQ, Pan L-L, Bhatia M, Sun J. Sulforaphane Protects Pancreatic Acinar Cell Injury by Modulating Nrf2-Mediated Oxidative Stress and NLRP3 Inflammatory Pathway. Oxid Med Cell Longev 2016;2016. https://doi.org/10.1155/2016/7864150.

[48] Sidhapuriwala JN, Hegde A, Ang AD, Zhu YZ, Bhatia M. Effects of S-propargyl-cysteine (SPRC) in caerulein-induced acute pancreatitis in mice. PLoS One 2012;7:e32574. https://doi.org/10.1371/journal.pone.0032574.

[49] Mathan Kumar M, Tamizhselvi R. Protective effect of diallyl disulfide against cerulein-induced acute pancreatitis and associated lung injury in mice. Int Immunopharmacol 2020;80:106136. https://doi.org/10.1016/j.intimp.2019.106136.

[50] Petrikovics I, Kiss L, Chou C-E, Ebrahimpour A, Kovács K, Kiss M, et al. Antidotal efficacies of the cyanide antidote candidate dimethyl trisulfide alone and in combination with cobinamide derivatives. Toxicol Mech Methods 2019;29:438–44. https://doi.org/10.1080/15376516.2019.1585504.

[51] Dong X, Kiss L, Petrikovics I, Thompson DE. Reaction of Dimethyl Trisulfide with Hemoglobin. Chem Res Toxicol 2017;30:1661–3. https://doi.org/10.1021/acs.chemrestox.7b00181.

[52] Bátai IZ, Dombi Á, Borbély É, Fehér Á, Papp F, Varga Z, et al. Investigation of the Role of the TRPA1 Ion Channel in Conveying the Effect of Dimethyl Trisulfide on Vascular and Histological Changes in Serum-Transfer Arthritis. Pharmaceuticals (Basel) 2022;15. https://doi.org/10.3390/ph15060671.

[53] Pozsgai G, Payrits M, Sághy É, Sebestyén-Bátai R, Steen E, Szőke É, et al. Analgesic effect of dimethyl trisulfide in mice is mediated by TRPA1 and sst4 receptors. Nitric Oxide 2017;65:10–21. https://doi.org/10.1016/j.niox.2017.01.012.

[54] Chandra-Kuntal K, Lee J, Singh S V. Critical role for reactive oxygen species in

apoptosis induction and cell migration inhibition by diallyl trisulfide, a cancer chemopreventive component of garlic. Breast Cancer Res Treat 2013;138:69–79. https://doi.org/10.1007/s10549-013-2440-2.

[55] Kuo W-W, Wang W-J, Tsai C-Y, Way C-L, Hsu H-H, Chen L-M. Diallyl trisufide (DATS) suppresses high glucose-induced cardiomyocyte apoptosis by inhibiting JNK/NFκB signaling via attenuating ROS generation. Int J Cardiol 2013;168:270–80. https://doi.org/10.1016/j.ijcard.2012.09.080.

[56] Silva-Islas CA, Chánez-Cárdenas ME, Barrera-Oviedo D, Ortiz-Plata A, Pedraza-Chaverri J, Maldonado PD. Diallyl Trisulfide Protects Rat Brain Tissue against the Damage Induced by Ischemia-Reperfusion through the Nrf2 Pathway. Antioxidants 2019;8:410. https://doi.org/10.3390/antiox8090410.

[57] Li L, Fox B, Keeble J, Salto-Tellez M, Winyard PG, Wood ME, et al. The complex effects of the slow-releasing hydrogen sulfide donor <scp>GYY</scp> 4137 in a model of acute joint inflammation and in human cartilage cells. J Cell Mol Med 2013;17:365–76. https://doi.org/10.1111/jcmm.12016.

[58] Lu S, Gao Y, Huang X, Wang X. GYY4137, a hydrogen sulfide (H_2S) donor, shows potent anti-hepatocellular carcinoma activity through blocking the STAT3 pathway. Int J Oncol 2014;44:1259–67. https://doi.org/10.3892/ijo.2014.2305.

[59] Lee ZW, Zhou J, Chen C-S, Zhao Y, Tan C-H, Li L, et al. The slow-releasing hydrogen sulfide donor, GYY4137, exhibits novel anti-cancer effects in vitro and in vivo. PLoS One 2011;6:e21077. https://doi.org/10.1371/journal.pone.0021077.

[60] Szczesny B, Módis K, Yanagi K, Coletta C, Le Trionnaire S, Perry A, et al. AP39, a novel mitochondria-targeted hydrogen sulfide donor, stimulates cellular bioenergetics, exerts cytoprotective effects and protects against the loss of mitochondrial DNA integrity in oxidatively stressed endothelial cells in vitro. Nitric Oxide 2014;41:120–30. https://doi.org/10.1016/j.niox.2014.04.008.

[61] Drucker NA, Jensen AR, Ferkowicz M, Markel TA. Hydrogen sulfide provides intestinal protection during a murine model of experimental necrotizing enterocolitis. J Pediatr Surg 2018;53:1692–8. https://doi.org/10.1016/j.jpedsurg.2017.12.003.

[62] Kauffman G. Aspirin-induced gastric mucosal injury: lessons learned from animal models. Gastroenterology 1989;96:606–14. https://doi.org/10.1016/s0016-5085(89)80056-3.

[63] Bjarnason I, Scarpignato C, Takeuchi K, Rainsford KD. Determinants of the short-term gastric damage caused by NSAIDs in man. Aliment Pharmacol Ther 2007;26:95–106. https://doi.org/10.1111/j.1365-2036.2007.03348.x.

[64] Kodela R, Chattopadhyay M, Kashfi K. NOSH-Aspirin: A Novel Nitric Oxide-Hydrogen Sulfide-Releasing Hybrid: A New Class of Anti-inflammatory Pharmaceuticals. ACS Med Chem Lett 2012;3:257–62. https://doi.org/10.1021/ml300002m.

[65] Campolo M, Esposito E, Ahmad A, Di Paola R, Paterniti I, Cordaro M, et al. Hydrogen sulfide-releasing cyclooxygenase inhibitor ATB-346 enhances motor function and reduces cortical lesion volume following traumatic brain injury in mice. J Neuroinflammation 2014;11:196. https://doi.org/10.1186/s12974-014-0196-1.

[66] Dief AE, Mostafa DK, Sharara GM, Zeitoun TH. Hydrogen sulfide releasing naproxen offers better anti-inflammatory and chondroprotective effect relative to naproxen in a rat model of zymosan induced arthritis. Eur Rev Med Pharmacol Sci 2015;19:1537–46.
[67] Wallace JL, Nagy P, Feener TD, Allain T, Ditrói T, Vaughan DJ, et al. A proof-of-concept, Phase 2 clinical trial of the gastrointestinal safety of a hydrogen sulfide-releasing anti-inflammatory drug. Br J Pharmacol 2020;177:769–77. https://doi.org/10.1111/bph.14641.
[68] Glanville JRW, Jalali P, Flint JD, Patel AA, Maini AA, Wallace JL, et al. Potent anti-inflammatory effects of an H $_2$ S-releasing naproxen (ATB-346) in a human model of inflammation. The FASEB Journal 2021;35. https://doi.org/10.1096/fj.201902918RR.
[69] Fűr G, Bálint ER, Orján EM, Balla Z, Kormányos ES, Czira B, et al. Mislocalization of CFTR expression in acute pancreatitis and the beneficial effect of VX-661 + VX-770 treatment on disease severity. J Physiol 2021;599:4955–71. https://doi.org/10.1113/JP281765.
[70] Lowry OH, Rosebrough NJ, Farr AL, Randall RJ. Protein measurement with the Folin phenol reagent. J Biol Chem 1951;193:265–75.
[71] John A. Williams. Isolation of rodent pancreatic acinar cells and acini by collagenase digestion. The Pancreapedia: Exocrine Pancreas Knowledge Base 2010. https://doi.org/10.3998/panc.2010.18.
[72] Akaike T, Ida T, Wei F-Y, Nishida M, Kumagai Y, Alam MM, et al. Cysteinyl-tRNA synthetase governs cysteine polysulfidation and mitochondrial bioenergetics. Nat Commun 2017;8:1177. https://doi.org/10.1038/s41467-017-01311-y.
[73] Dóka É, Ida T, Dagnell M, Abiko Y, Luong NC, Balog N, et al. Control of protein function through oxidation and reduction of persulfidated states. Sci Adv 2020;6. https://doi.org/10.1126/sciadv.aax8358.
[74] Czikora Á, Erdélyi K, Ditrói T, Szántó N, Jurányi EP, Szanyi S, et al. Cystathionine β-synthase overexpression drives metastatic dissemination in pancreatic ductal adenocarcinoma via inducing epithelial-to-mesenchymal transformation of cancer cells. Redox Biol 2022;57:102505. https://doi.org/10.1016/j.redox.2022.102505.
[75] Erdélyi K, Ditrói T, Johansson HJ, Czikora Á, Balog N, Silwal-Pandit L, et al. Reprogrammed transsulfuration promotes basal-like breast tumor progression via realigning cellular cysteine persulfidation. Proceedings of the National Academy of Sciences 2021;118. https://doi.org/10.1073/pnas.2100050118.
[76] Gerasimenko J V, Petersen OH, Gerasimenko O V. SARS-CoV-2 S Protein Subunit 1 Elicits Ca2+ Influx - Dependent Ca2+ Signals in Pancreatic Stellate Cells and Macrophages In Situ. Function (Oxf) 2022;3:zqac002. https://doi.org/10.1093/function/zqac002.
[77] Gerasimenko J V, Gerasimenko O V. The role of Ca2+ signalling in the pathology of exocrine pancreas. Cell Calcium 2023;112:102740. https://doi.org/10.1016/j.ceca.2023.102740.
[78] Powell CR, Dillon KM, Matson JB. A review of hydrogen sulfide (H2S) donors: Chemistry and potential therapeutic applications. Biochem Pharmacol 2018;149:110–

23. https://doi.org/10.1016/j.bcp.2017.11.014.
[79] Iciek M, Bilska-Wilkosz A, Górny M. Sulfane sulfur - new findings on an old topic. Acta Biochim Pol 2019;66:533–44. https://doi.org/10.18388/abp.2019_2909.
[80] Kang JS, Kim G-Y, Kim BW, Choi YH. Antioxidative effects of diallyl trisulfide on hydrogen peroxide-induced cytotoxicity through regulation of nuclear factor-E2-related factor-mediated thioredoxin reductase 1 expression in C2C12 skeletal muscle myoblast cells. Gen Physiol Biophys 2017;36:129–39. https://doi.org/10.4149/gpb_2016042.
[81] Zhang F, Jin H, Wu L, Shao J, Zhu X, Chen A, et al. Diallyl Trisulfide Suppresses Oxidative Stress-Induced Activation of Hepatic Stellate Cells through Production of Hydrogen Sulfide. Oxid Med Cell Longev 2017;2017:1406726. https://doi.org/10.1155/2017/1406726.
[82] Gryshchenko O, Gerasimenko J V, Petersen OH, Gerasimenko O V. Calcium Signaling in Pancreatic Immune Cells *In situ*. Function 2020;2. https://doi.org/10.1093/function/zqaa026.
[83] Mustafa AK, Gadalla MM, Sen N, Kim S, Mu W, Gazi SK, et al. H2S signals through protein S-sulfhydration. Sci Signal 2009;2:ra72. https://doi.org/10.1126/scisignal.2000464.
[84] Paul BD, Snyder SH. H2S signalling through protein sulfhydration and beyond. Nat Rev Mol Cell Biol 2012;13:499–507. https://doi.org/10.1038/nrm3391.
[85] Mishanina T V, Libiad M, Banerjee R. Biogenesis of reactive sulfur species for signaling by hydrogen sulfide oxidation pathways. Nat Chem Biol 2015;11:457–64. https://doi.org/10.1038/nchembio.1834.
[86] Wang H, Shi X, Qiu M, Lv S, Liu H. Hydrogen Sulfide Plays an Important Protective Role through Influencing Endoplasmic Reticulum Stress in Diseases. Int J Biol Sci 2020;16:264–71. https://doi.org/10.7150/ijbs.38143.
[87] Lo Faro ML, Fox B, Whatmore JL, Winyard PG, Whiteman M. Hydrogen sulfide and nitric oxide interactions in inflammation. Nitric Oxide 2014;41:38–47. https://doi.org/10.1016/j.niox.2014.05.014.
[88] Ditrói T, Nagy A, Martinelli D, Rosta A, Kožich V, Nagy P. Comprehensive analysis of how experimental parameters affect H2S measurements by the monobromobimane method. Free Radic Biol Med 2019;136:146–58. https://doi.org/10.1016/j.freeradbiomed.2019.04.006.
[89] Nagy P, Dóka É, Ida T, Akaike T. Measuring Reactive Sulfur Species and Thiol Oxidation States: Challenges and Cautions in Relation to Alkylation-Based Protocols. Antioxid Redox Signal 2020;33:1174–89. https://doi.org/10.1089/ars.2020.8077.
[90] Bogdándi V, Ida T, Sutton TR, Bianco C, Ditrói T, Koster G, et al. Speciation of reactive sulfur species and their reactions with alkylating agents: do we have any clue about what is present inside the cell? Br J Pharmacol 2019;176:646–70. https://doi.org/10.1111/bph.14394.
[91] Qiu Y, Wu Y, Meng M, Luo M, Zhao H, Sun H, et al. GYY4137 protects against myocardial ischemia/reperfusion injury via activation of the PHLPP-1/Akt/Nrf2 signaling pathway in diabetic mice. Journal of Surgical Research 2018;225:29–39.

https://doi.org/10.1016/j.jss.2017.12.030.
[92] Chen X, Liu X. Hydrogen sulfide from a NaHS source attenuates dextran sulfate sodium (DSS)-induced inflammation via inhibiting nuclear factor-κB. Journal of Zhejiang University-SCIENCE B 2016;17:209–17. https://doi.org/10.1631/jzus.B1500248.
[93] Xu W, Wu W, Chen J, Guo R, Lin J, Liao X, et al. Exogenous hydrogen sulfide protects H9c2 cardiac cells against high glucose-induced injury by inhibiting the activities of the p38 MAPK and ERK1/2 pathways. Int J Mol Med 2013;32:917–25. https://doi.org/10.3892/ijmm.2013.1462.
[94] Lu W, Mao Y, Cai S, Chen Q, Xu P, Xu C, et al. Identification and mechanistic analysis of shared biomarkers and pathogenesis in acute pancreatitis and sepsis based on differential gene expression and protein interaction networks. Funct Integr Genomics 2025;25:90. https://doi.org/10.1007/s10142-025-01600-6.
[95] Yan M-X, Li Y-Q, Meng M, Ren H-B, Kou Y. Long-term high-fat diet induces pancreatic injuries via pancreatic microcirculatory disturbances and oxidative stress in rats with hyperlipidemia. Biochem Biophys Res Commun 2006;347:192–9. https://doi.org/10.1016/j.bbrc.2006.06.063.
[96] Zhang F, Sun Y, Fan K, Dong X, Han N, Zhao H, et al. Protective effects of heme oxygenase-1 against severe acute pancreatitis via inhibition of tumor necrosis factor-α and augmentation of interleukin-10. BMC Gastroenterol 2017;17:100. https://doi.org/10.1186/s12876-017-0651-4.
[97] Xi C, Pang J, Xue W, Cui Y, Jiang N, Zhi W, et al. Transsulfuration pathway activation attenuates oxidative stress and ferroptosis in sickle primary erythroblasts and transgenic mice. Commun Biol 2025;8:15. https://doi.org/10.1038/s42003-024-07424-7.
[98] Farmer LA, Wu Z, Poon J-F, Zilka O, Lorenz SM, Huehn S, et al. Intrinsic and Extrinsic Limitations to the Design and Optimization of Inhibitors of Lipid Peroxidation and Associated Cell Death. J Am Chem Soc 2022;144:14706–21. https://doi.org/10.1021/jacs.2c05252.
[99] Mallais M, Hanson CS, Giray M, Pratt DA. General Approach to Identify, Assess, and Characterize Inhibitors of Lipid Peroxidation and Associated Cell Death. ACS Chem Biol 2023;18:561–71. https://doi.org/10.1021/acschembio.2c00897.
[100] Latunde-Dada GO. Ferroptosis: Role of lipid peroxidation, iron and ferritinophagy. Biochimica et Biophysica Acta (BBA) - General Subjects 2017;1861:1893–900. https://doi.org/10.1016/j.bbagen.2017.05.019.
[101] Lu J, Holmgren A. The thioredoxin antioxidant system. Free Radic Biol Med 2014;66:75–87. https://doi.org/10.1016/j.freeradbiomed.2013.07.036.
[102] Tang D, Chen X, Kang R, Kroemer G. Ferroptosis: molecular mechanisms and health implications. Cell Res 2021;31:107–25. https://doi.org/10.1038/s41422-020-00441-1.
[103] Maiorino M, Conrad M, Ursini F. GPx4, Lipid Peroxidation, and Cell Death: Discoveries, Rediscoveries, and Open Issues. Antioxid Redox Signal 2018;29:61–74. https://doi.org/10.1089/ars.2017.7115.
[104] Wang M, Tang J, Zhang S, Pang K, Zhao Y, Liu N, et al. Exogenous H2S initiating Nrf2/GPx4/GSH pathway through promoting Syvn1-Keap1 interaction in diabetic

hearts. Cell Death Discov 2023;9:394. https://doi.org/10.1038/s41420-023-01690-w.